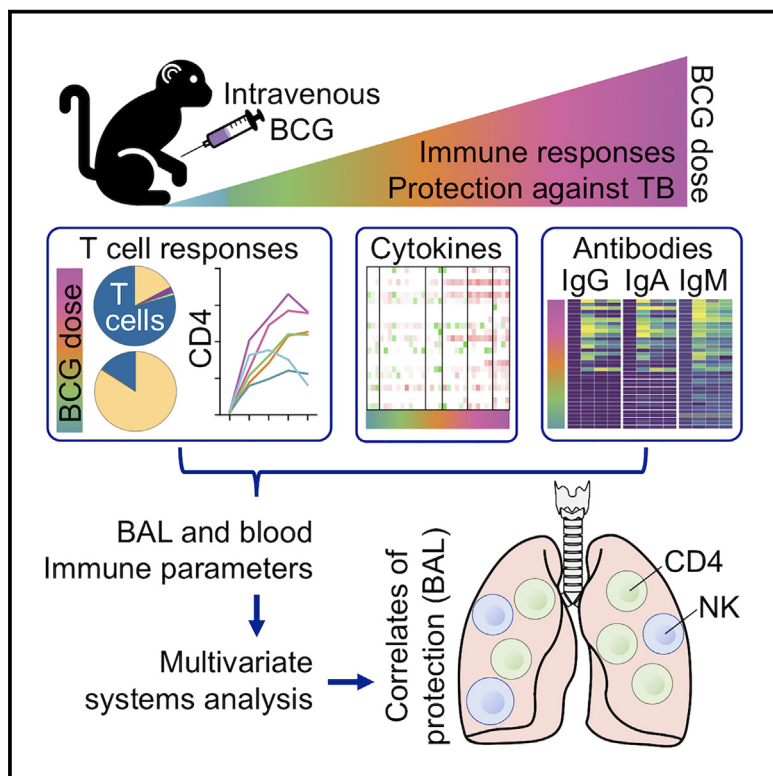


Cell Host & Microbe

Airway T cells are a correlate of i.v. Bacille Calmette-Guerin-mediated protection against tuberculosis in rhesus macaques

Graphical abstract



Authors

Patricia A. Darrah, Joseph J. Zeppa, Chuangqi Wang, ..., Robert A. Seder, Pauline Maiello, Mario Roederer

Correspondence

marior@mail.nih.gov

In brief

Vaccination with intravenous Bacille Calmette-Guerin (i.v. BCG) protects macaques from tuberculosis. Using a dose-ranging i.v. BCG strategy, Darrah, Zeppa, Wang, et al. elicited graded immune responses and 50% protection in macaques. Multivariate analysis of longitudinal cellular and humoral parameters identified antigen-specific CD4 T cells and NK cells in the airway as strong correlates of protection.

Highlights

- An i.v. Bacille Calmette-Guerin (BCG) dose-ranging study generated a range of protection against tuberculosis in macaques
- Immune measurements from blood and BAL were integrated for correlates analysis
- Multivariate analysis of BAL features revealed a highly coordinated immune network
- Tuberculosis-specific CD4 Th1/Th17 and NK cells in the airway correlated with protection



Article

Airway T cells are a correlate of i.v. Bacille Calmette-Guerin-mediated protection against tuberculosis in rhesus macaques

Patricia A. Darrah,^{1,9} Joseph J. Zeppa,^{2,9} Chuangqi Wang,^{3,8,9} Edward B. Irvine,^{4,7} Allison N. Bucsan,¹ Mark A. Rodgers,² Supriya Pokkali,¹ Joshua A. Hackney,¹ Megha Kamath,¹ Alexander G. White,² H. Jacob Borish,² L. James Frye,² Jaime Tomko,² Kara Kracinovsky,² Philana Ling Lin,⁵ Edwin Klein,⁶ Charles A. Scanga,² Galit Alter,⁴ Sarah M. Fortune,^{4,7} Douglas A. Lauffenburger,⁸ JoAnne L. Flynn,² Robert A. Seder,¹ Pauline Maiello,^{2,10} and Mario Roederer^{1,10,11,*}

¹Vaccine Research Center, National Institute of Allergy and Infectious Diseases, National Institutes of Health, Bethesda, MD 20892, USA

²Department of Microbiology and Molecular Genetics, University of Pittsburgh School of Medicine and Center for Vaccine Research, University of Pittsburgh, Pittsburgh, PA 15261, USA

³Department of Immunology and Microbiology, University of Colorado, Anschutz Medical Campus, Aurora, CO 80045, USA

⁴Ragon Institute of Massachusetts General Hospital, MIT and Harvard, Cambridge, MA 02139, USA

⁵Department of Pediatrics, University of Pittsburgh School of Medicine, UPMC Children's Hospital of Pittsburgh, and Center for Vaccine Research, University of Pittsburgh, Pittsburgh, PA 15620, USA

⁶Division of Animal Laboratory Resources, University of Pittsburgh School of Medicine, Pittsburgh, PA 15261, USA

⁷Department of Immunology and Infectious Diseases, Harvard T.H. Chan School of Public Health, Boston, MA 02115, USA

⁸Department of Biological Engineering, Massachusetts Institute of Technology, Cambridge, MA 02142, USA

⁹These authors contributed equally

¹⁰Senior author

¹¹Lead contact

*Correspondence: marior@mail.nih.gov

<https://doi.org/10.1016/j.chom.2023.05.006>

SUMMARY

Bacille Calmette-Guerin (BCG), the only approved *Mycobacterium tuberculosis* (Mtb) vaccine, provides limited durable protection when administered intradermally. However, recent work revealed that intravenous (i.v.) BCG administration yielded greater protection in macaques. Here, we perform a dose-ranging study of i.v. BCG vaccination in macaques to generate a range of immune responses and define correlates of protection. Seventeen of 34 macaques had no detectable infection after Mtb challenge. Multivariate analysis incorporating longitudinal cellular and humoral immune parameters uncovered an extensive and highly coordinated immune response from the bronchoalveolar lavage (BAL). A minimal signature predicting protection contained four BAL immune features, of which three remained significant after dose correction: frequency of CD4 T cells producing TNF with interferon γ (IFN γ), frequency of those producing TNF with IL-17, and the number of NK cells. Blood immune features were less predictive of protection. We conclude that CD4 T cell immunity and NK cells in the airway correlate with protection following i.v. BCG.

INTRODUCTION

Tuberculosis (TB) is a leading cause of death from infection worldwide, and approximately 25% of the world's population has asymptomatic *Mycobacterium tuberculosis* (Mtb) infection (latent TB infection, LTBI), which can reactivate and cause transmissible pulmonary TB disease. Treatment for active TB requires lengthy drug regimens that can lead to limited compliance, and an increasing prevalence of drug-resistant TB complicates therapy. The only approved vaccine, live-attenuated Bacille Calmette-Guerin (BCG), was developed 100 years ago and is administered intradermally (ID) at birth in most TB-endemic countries. Although ID BCG reduces the incidence of disseminated TB in infancy and early childhood, it has limited durable protection against pulmonary TB in adolescents

and adults.¹ As pulmonary TB accounts for most of the morbidity, mortality, and transmission, a major goal is to limit pulmonary TB disease in adolescents and adults.

Mtb is transmitted by the aerosol route and initiates infection in alveolar macrophages. Antibodies could limit early Mtb replication within macrophages or modulate immune responses to Mtb.² Once the infection is established, however, T cell immunity is required to control replication and limit TB disease and reactivation. Experiments have shown that CD4 T cells, interferon γ (IFN γ), and tumor necrosis factor (TNF) are important for protection by vaccines.³ These data are substantiated in humans with genetic deficiencies of IFN γ and interleukin (IL)-12 signaling and in those treated with biologics that neutralize TNF.^{4,5} TB is the major cause of death in HIV-infected individuals, which is associated with a loss of CD4 T cell responses.



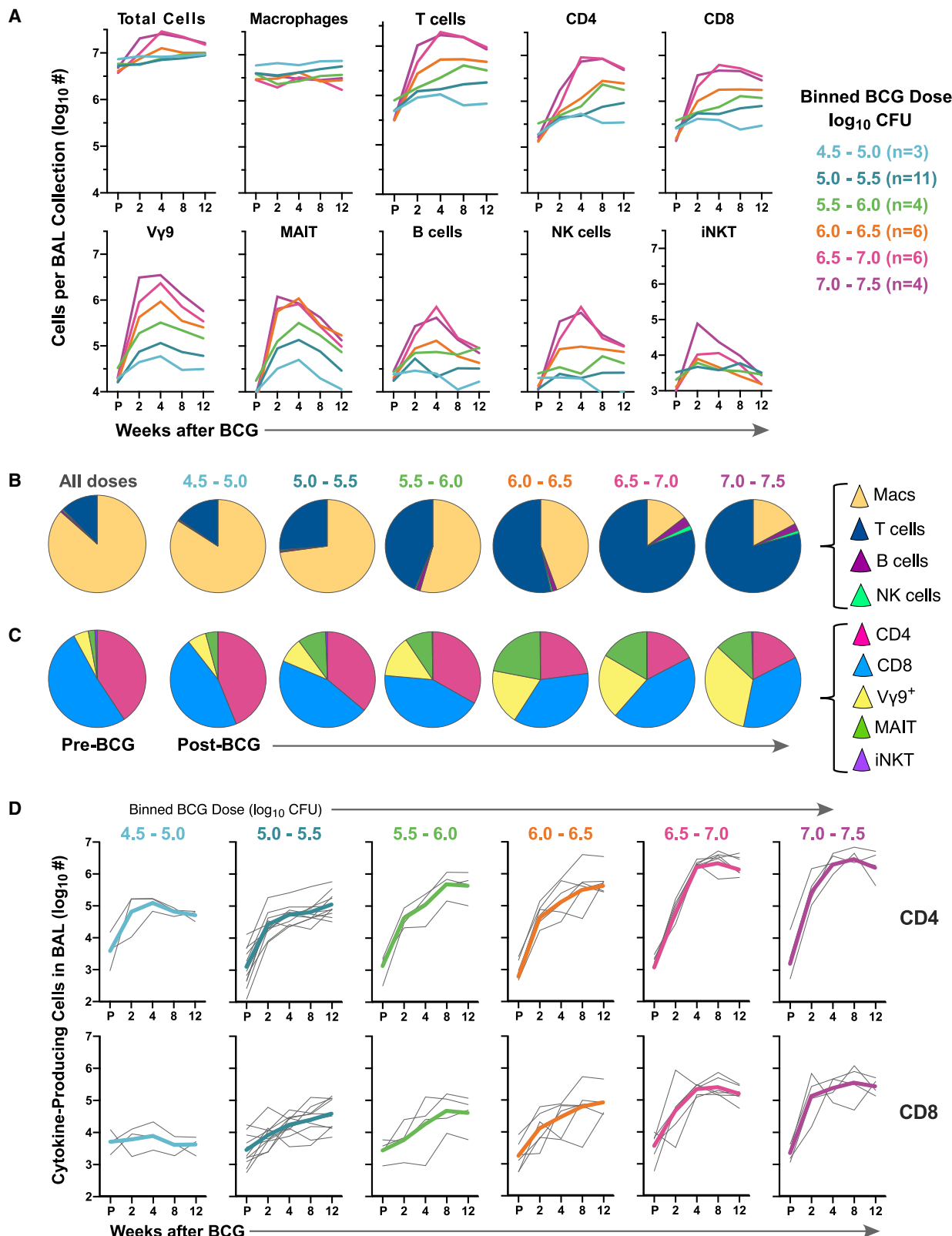


Figure 1. Serial assessment of the total cells and mycobacterial-specific T cells in BAL after varied i.v. BCG vaccination doses

Rhesus macaques were vaccinated with half-log increasing doses of i.v. BCG between 4.5 and 7.5 \log_{10} CFU; binned dose groups (with number of animals per bin) are color coded. BAL was collected before (Pre; P) and 2, 4, 8, and 12 weeks after vaccination.

Other immune cells implicated in TB immunity in animal models include CD4 Th17 cells, CD8 T cells, and donor-unrestricted cells such as $\gamma\delta$ T cells, mucosal-associated invariant T (MAIT) cells, and natural killer (NK) cells.⁶ Until recently,^{7–10} there have been no preclinical vaccine models that show high-level protection against TB infection or disease, which are important for defining correlates and mechanisms for preventing infection.

We previously showed that intravenous (i.v.) BCG immunization protected 9 out of 10 rhesus macaques against *Mtb* challenge, which contrasted to limited protection afforded by ID or aerosol BCG administered at the same dose.⁷ Of note, 6 of the 9 protected animals had no detectable *Mtb* post-challenge, suggesting that i.v. BCG could mediate sterilizing protection. Thus, i.v. BCG provides a model to define immune correlates of protection for the prevention of infection and disease. Analysis of bronchoalveolar lavage (BAL) and lung tissue after i.v. BCG revealed a substantial increase in antigen-specific CD4 T cells with a unique Th1/Th17 transcriptional signature.⁷ Additionally, i.v. BCG elicited antigen-specific CD8 T cells as well as broad IgG, IgA, and IgM antibody responses.^{7,11} However, since 90% of i.v. BCG-immunized animals were protected against disease, we were unable to discern innate, cellular, or humoral correlates of protection among these animals. Thus, it remains to be determined which among these possibilities might be the strongest correlates.

Here, we performed a dose-ranging study of i.v. BCG in rhesus macaques, hypothesizing that we would generate a wide range of immune responses and protective outcomes facilitating immune correlates analysis. We assessed a large number of innate, cellular, and humoral immune responses over time after vaccination and used multivariate modeling to identify correlates of protection from blood and BAL samples. We pre-specified four immune measurements to query as prognostic correlates of protection, i.e., the number and frequency of antigen-specific CD4 and CD8 T cells in BAL (airway). In addition, we performed an extensive exploratory multivariate analysis encompassing a wide range of immune phenotypes and functions. We show that adaptive cellular immune correlates of protection are preferentially defined in the airway (the site of infection) compared with the blood. In a separate analysis (*Cell Reports Medicine*, accepted for upcoming publication), Liu et al. analyzed the blood-derived transcriptomics from the same study and discovered an early innate signature that predicted the generation of adaptive BAL immune features associated with protection, as well as protection directly. These data will direct future vaccine designs to elicit such lung-localized adaptive immune responses and guide the analysis of clinical trials aimed at eliciting protection against TB.

RESULTS

Experimental design and safety

This study was designed to determine the immune correlates of i.v. BCG-mediated protection against TB in rhesus macaques by using a range of BCG doses to achieve 50% protective efficacy—which is optimal for correlates analysis. Thirty-four rhesus macaques were immunized with i.v. BCG; we administered approximately half-log decreasing doses between a highly protective dose of 2.5×10^7 ($7.4 \log_{10}$) and 3.9×10^4 ($4.6 \log_{10}$) colony forming units (CFU) (Figure S1A). This study (with varied group sizes) was not designed to perform detailed statistical comparisons between dose groups but rather to use different doses to generate a range of immune responses and protection. Immune responses in blood and BAL were assessed up to 24 weeks following immunization, after which animals were challenged with *Mtb* Erdman (4–17 CFU) and monitored for TB disease using positron-emission tomography-computed tomography (PET CT) imaging (Figure S1B). Necropsies were done 12 weeks post-challenge or when animals had substantial disease determined by PET CT scans or clinical signs, reaching humane endpoints. A complete summary of all animals used in this study, along with doses of BCG and *Mtb* administered, is shown in (Table S1).

To assess safety, plasma cytokines, C-reactive protein (CRP), and clinical parameters (temperature, weight, complete blood counts, and serum chemistries) were measured after i.v. BCG administration (Figure S2). Not only serum proteins associated with inflammation and Th1 T cell induction, including IL-8, sCD40L, MCP-1, IL-6, IL-12, and IL-18 but also anti-inflammatory cytokines, such as IL-10 and IL-1RA, were increased between 6 h and 7 days after vaccination and were largely influenced by the BCG dose (Figure S2A). Neutrophil and monocyte counts, as well as aspartate aminotransferase (AST) and creatine phosphokinase (CPK), were transiently increased at 6 h after vaccination, whereas CRP was elevated for 7–14 days at higher i.v. BCG doses before returning to normal (Figure S2B). No increases in the temperature were observed.

Leukocyte composition in BAL and blood after i.v. BCG vaccination

Previously, vaccination with a high dose ($7.64 \log_{10}$ CFU) of i.v. BCG resulted in a large and sustained influx of T cells into the BAL.⁷ Here, following i.v. BCG, the median influx of T cells, B cells, and NK cells into the BAL was dose-responsive (Figure 1A). Animals vaccinated with the lowest doses of i.v. BCG displayed no detectable changes in BAL leukocyte numbers (Figure S4A). In contrast and consistent with our prior data, higher doses of i.v. BCG (6.0 – $7.5 \log_{10}$ CFU) resulted in 10- to 30-fold increases in CD4 and CD8 T cells—substantially altering the proportions of

(A) Geometric mean number (\log_{10}) of the total cells (live, nucleated cell counts) or selected leukocyte subsets (identified by flow cytometry) in the BAL before and after i.v. BCG are shown for each binned dose group. See also Figures S3 and S4A.

(B and C) Average proportions of indicated live leukocyte (B) or CD3⁺ T cell (C) subset in BAL for animals in each dose group at 2–4 weeks after i.v. BCG. See also Figures S4B and S4C.

(D) Number (\log_{10}) of memory CD4 (top) or CD8 (bottom) T cells in BAL producing IFN γ , IL-2, TNF, or IL-17 following *in vitro* stimulation with mycobacterial antigens (purified protein derivative; PPD) as identified by flow cytometry. Shown are individual (thin gray lines) and median (thick colored lines) responses for macaques in each dose group before and after i.v. BCG. See also Figures S6 and S7.

T cells and macrophages in the BAL (Figures 1B and S4B) for at least 12 weeks after vaccination. Transient increases in the absolute numbers (Figure 1A) and proportions (Figures 1C and S4C) of donor-unrestricted T cells (i.e., V γ 9 $^+$ γ δ T cells and MAIT cells) were observed in BAL 2 to 4 weeks after vaccination in a dose-dependent manner.

A more extensive longitudinal flow cytometric analysis of leukocyte composition was assessed from PBMC (Figure S5). Although the overall proportion of the total T cells was not affected following i.v. BCG vaccination (Figure S4D), the proportions of CD3 $^+$ T cells that were V γ 9 $^+$ γ δ T cells and MAIT cells increased with higher i.v. BCG doses between 2 and 4 weeks after vaccination (Figure S4E). In general, the pattern of immune alterations following i.v. BCG was dose-dependent and more profound in BAL than in the blood.

Antigen-specific T cell responses in BAL and blood after i.v. BCG

A primary goal of this study was to generate quantitatively or qualitatively different immune responses across animals by varying the vaccine dose. The magnitude and quality of T cell cytokine responses following *ex vivo* restimulation with mycobacterial antigens (tuberculin purified protein derivative; PPD) were assessed in BAL. We identified antigen-specific T cells producing any combination of IFN γ , IL-2, TNF, or IL-17, the canonical Th1/Th17 associated cytokines shown to be important for protection against TB in various animal models and humans.^{6,8,12–20}

Macaques from all dose groups generated antigen-specific CD4 T cells in BAL that generally peaked between 8 and 12 weeks after vaccination (Figures 1D and S7A). Depending on the i.v. BCG dose, CD4 T cell responses in the BAL increased 10-fold to 1000-fold in number (Figure 1D) following vaccination, yielding peak IFN γ or TNF frequencies of >50% of all memory CD4 T cells (Figure S7A). Cytokine-producing CD8 T cells in the BAL were lower and more variable in both number and frequency than CD4 T cells, particularly at the lower i.v. BCG doses (Figures 1D and S7D).

Although the absolute frequencies of cytokine-positive T cells in the BAL varied with BCG dose (Figures S7A and S7D), qualitatively, the relative proportions of IFN γ , IL-2, or TNF production (in any combination) by CD4 (Figure S7B) or CD8 (Figure S7E) T cells was similar across i.v. BCG doses. Compared with the frequencies of canonical CD4 Th1 cytokines (IFN γ , TNF, or IL-2), IL-17 production was substantially lower (Figures S7A and S7C), comprising <10% of the total peak CD4 T cell response (Figure S7B, black pie arcs). The profile of IFN γ , IL-2, and TNF expressions by IL-17 $^+$ versus IL-17 $^-$ CD4 T cells was similar (Figure S7C, pies).

For the analysis of antigen-specific T cell responses in PBMCs, we applied a more extensive flow cytometry panel (Figure S8) that measured IFN γ , IL-2, TNF, and IL-17 production as well as additional T cell markers, including the activation-induced markers CD154 and CD153, and the cytotoxic markers CD107a and granzyme B. Although all i.v. BCG dose groups had detectable CD4 and CD8 T responses to mycobacterial antigens (Mtb whole cell lysate; WCL), the magnitude of responses in PBMC (Figures 2A and S9A) was far lower than that measured in BAL (Figure S7A). CD4 T cells from PBMC of matched dose groups produced similar frequencies of IFN γ , TNF, and CD154

but lower frequencies of IL-2, CD153, and particularly IL-17 (Figure S9A). Like the BAL, the quality of the CD4 T cell cytokine response (proportion of cells producing any combination of CD154, IFN γ , IL-2, TNF, or IL-17) in PBMC was similar across i.v. BCG dose groups (Figure S9C). Essentially, all cytokine-producing cells expressed CD154, a sensitive marker of antigen-specific CD4 T cell activation. CD8 T cells and V γ 9 $^+$ γ δ T cells produced mainly IFN γ and TNF following stimulation (Figures S9D, S9F, and S9G) and a higher proportion of the cytolytic markers CD107a and granzyme B compared with CD4 T cells (Figures S9B, S9E, and S9H). PBMC IFN γ enzyme-linked immunosorbent spots (ELISpots) against mycobacterial antigens (culture filtrate protein; CFP), which may represent CD4 or CD8 T cells, also showed a dose-dependent response at the time of challenge (Figure 2B).

Antigen-specific antibody responses in blood and BAL after i.v. BCG

Prior studies demonstrated that high-dose i.v. BCG vaccination induced mycobacterial-specific antibody responses and that IgM titers in BAL and plasma were associated with protection.¹¹ Hence, we next sought to define the influence of i.v. BCG dose on humoral immunity. IgG1, IgA, and IgM antibody titers to two mycobacterial antigens (lipoarabinomannan; LAM, and PPD) were evaluated longitudinally before and after BCG immunization in plasma and BAL using a custom Luminex assay (Figure 3).²¹

In plasma (Figures 3A–3C), LAM-specific IgG1, IgA, and IgM titers peaked 4 weeks after vaccination and, in some animals that received high-dose i.v. BCG, remained elevated until the time of Mtb challenge (24 weeks). Conversely, LAM-specific antibody titers from macaques in lower BCG dose groups waned over time (Figure 3A). PPD-specific antibody titers in plasma were modest overall with IgG1 titers that peaked 4 weeks after BCG (Figure 3B). LAM-specific IgG1 and IgM and PPD-specific IgM titers in plasma correlated with the i.v. BCG dose (Figure 3C), indicating the potential for using select humoral measurements in the periphery as markers of i.v. BCG vaccination dose.

Antibody profiling in BAL fluid (Figures 3D–3F) revealed increases in LAM-specific IgG1, IgA, and IgM at 4 weeks that persisted up to 12 weeks following immunization in macaques from higher i.v. BCG dose groups (Figure 3D). PPD-specific antibody responses emerged 4 weeks following vaccination in higher dose groups but were relatively low (Figure 3E). Animals in the lower BCG dose groups displayed minimal antibody responses to LAM or PPD in BAL. BAL antibody measurements were strongly co-correlated (Figure 3F), indicating a coordinated humoral immune response in the airway triggered by i.v. BCG vaccination. As a result (and in contrast to plasma), every antibody feature from BAL correlated with i.v. BCG dose (Figure 3F). Together, these data demonstrate that i.v. BCG drives dose-dependent increases in LAM-specific IgG1 and LAM- and PPD-specific IgM in the periphery and at the site of the infection.

Protection against Mtb challenge following i.v. BCG vaccination

Six months after i.v. BCG immunization, macaques were challenged with a low dose (4–17 CFU) of Mtb Erdman. We

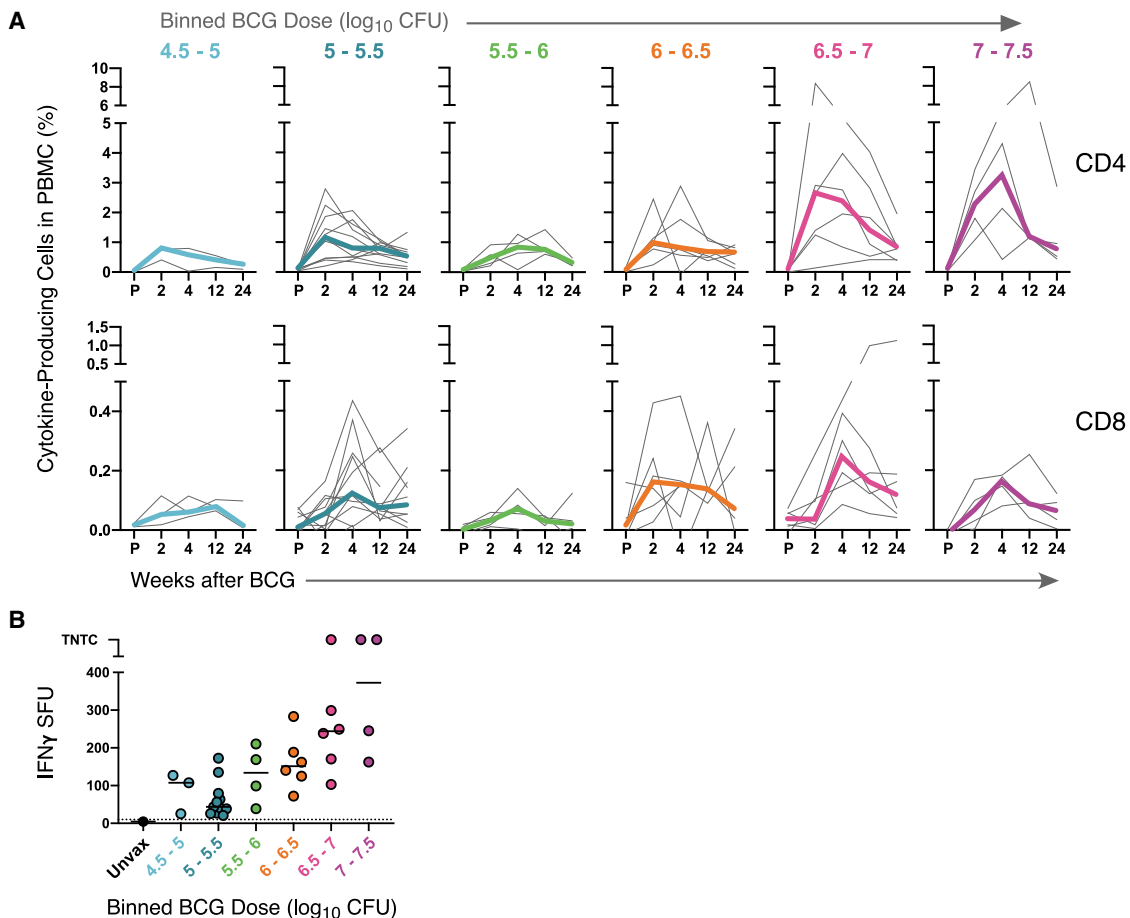


Figure 2. Mycobacterial-specific T cell responses in PBMC after varied i.v. BCG vaccination doses

(A) Frequency of memory CD4 (top) or CD8 (bottom) T cells in PBMC producing IFN γ , IL-2, TNF, or IL-17 following *in vitro* stimulation with mycobacterial antigens (whole cell lysate; WCL) as identified by flow cytometry. Shown are individual (thin gray lines) and median (thick colored lines) responses for macaques in each i.v. BCG binned dose group before (Pre, P) and 2, 4, 12, and 24 weeks after i.v. BCG. See also Figure S8 and S9.

(B) Number of IFN γ spot-forming units (SFU) per 200,000 cells in each dose group following stimulation of PBMC with mycobacterial antigens (culture filtrate protein, CFP) at the time of Mtb challenge (24 weeks); symbols represent individual animals and bars are medians.

pre-specified an endpoint of 12 weeks post-challenge, at which time, the animals underwent necropsy and extensive pathology and immune analysis (Figure S1B). TB disease was tracked longitudinally using ^{18}F -fluorodeoxyglucose (FDG) PET CT imaging; total FDG activity is a measure of cellular metabolism and inflammation that correlates with the total thoracic Mtb burden.^{22,23} As early as 4 weeks post-challenge, FDG activity in the lungs was increased in the unvaccinated control and in one or more animals from each of the lowest four i.v. BCG dose groups (\log_{10} 4.5–6.5) (Figure 4A). Throughout the entire post-challenge phase, 11 of 34 vaccinated macaques had measurable lung FDG activity, whereas 23 macaques, including all animals in the two highest dose groups (\log_{10} 6.5–7.5), had none (Figures 4A–4C). Whereas not all vaccinated macaques had granulomas observed by CT or found at necropsy, those macaques that had measurable lung FDG activity also had lung granulomas (Figure 4A). Although an axial view of scans is used to quantify FDG and identify granulomas, three-dimensional reconstructions of pre-necropsy PET CT scans provide a visual representation of TB disease in each macaque (Figure 4B).

The infection outcome measures at necropsy of lung inflammation (Figure 4C), number of granulomas (Figure 4D), total pathology score (Figure 4E), and lung pathology score (Figure 4F) show a moderate negative correlation with i.v. BCG dose (Kendall's τ and corresponding p value) indicating that i.v. BCG dose influences protection against Mtb infection and disease. Lymph node pathology (Figure 4G) and extrapulmonary (Figure 4H) scores were not significantly correlated with dose. At the highest dose (\log_{10} 7–7.5), these outcome measures were consistent with our previous study using a similar dose.⁷ Detailed necropsies revealed some sign of infection (i.e., one or more lung or lymph node granulomas) in at least one animal in each dose group (Figures 4D and 4G), with more animals showing TB-related pathology at the lower i.v. BCG doses.

The pre-defined primary outcome measure of protection was a comprehensive quantification of Mtb burden (CFU) at necropsy. All lung granulomas, other areas of lung pathology, all thoracic lymph nodes, and half of each grossly uninvolved lung were individually collected using the pre-necropsy PET CT scan as a map of the disease. Total thoracic CFU is the sum of

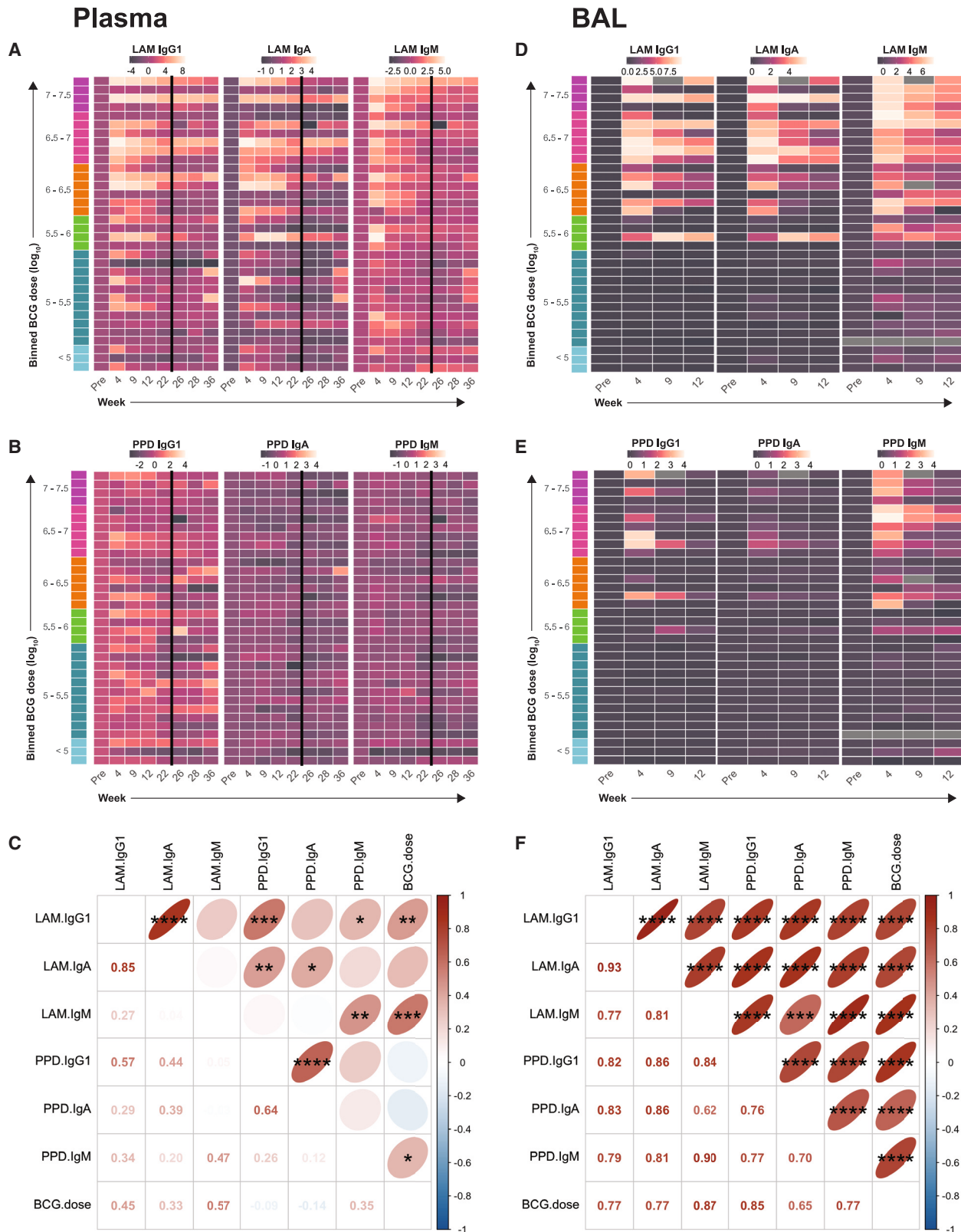


Figure 3. Mycobacterial-specific antibody responses in blood and BAL after varied i.v. BCG doses

(A and B) Heatmaps of lipoarabinomannan (LAM)- (A) and PPD- (B) specific IgG1, IgA, and IgM antibody titers in the plasma of individual macaques (ordered by binned dose group) following i.v. BCG vaccination and Mtb challenge (24 weeks).

all samples, reflecting a true thoracic bacterial burden for each animal. For three vaccinated animals with extensive disease, the total thoracic CFU was estimated using total FDG activity in the lung immediately before necropsy rather than by detailed necropsy (star-shaped symbols, *Figure 5A*). In most cases, macaques with lung CFU also had Mtb in the thoracic lymph nodes (*Figures 5B* and *5C*). One animal in the highest BCG dose group (\log_{10} 7–7.5) had <100 CFU in total (from a thoracic lymph node), whereas the three other animals in this dose group were sterile. Although there was a clear vaccine dose effect on total thoracic CFU ($\tau = -0.3585$, $p = 0.0066$), at least one animal from each i.v. BCG dose group had no detectable Mtb in the thoracic cavity, i.e., sterilizing immunity (*Figure 5A*). In summary, 17 of 34 animals across all doses showed sterilizing immunity (0 Mtb CFU), and 18 of 34 were considered protected (<100 Mtb CFU).

Interferon gamma release assay (IGRA) as a measure of Mtb infection

As commonly used to detect TB infection in humans, we performed a blood-based IGRA using Mtb-specific antigens that are not present in BCG (ESAT-6 and CFP-10). Thus, to provide an orthogonal assessment of infection with a translatable clinical test, we assessed Mtb infection by IFN γ ELISpot prior to challenge and at the time of necropsy (12 weeks post-Mtb) (*Figure 5D*). In this analysis, we categorized animals as sterile or non-sterile based on Mtb CFU at necropsy and defined positive ELISpot responses as >10 spot-forming units (SFU) per 200,000 PBMC (*Figure S10A*). The ELISpot assay was accurate at predicting infection (*Figure 5E*): of macaques with ESAT-6 + CFP-10 responses <10 SFU, 86.7% were sterile, whereas 13.3% of the animals were incorrectly identified as non-sterile. In macaques with >10 SFU, 78.9% were non-sterile and 21.1% were sterile. Thus, for total thoracic sterility, the IFN γ ELISpot assay had a sensitivity (ability to detect infected macaques) of 88.2% and a specificity (ability to detect uninfected macaques) of 76.5%. These data have implications for interpreting IGRA as a diagnostic marker of human Mtb infection. A similar analysis was done using lung and lung lymph node sterility (*Figure S10B*). Flow cytometry assays using ESAT-6 and CFP-10 peptide stimulations of PBMC before and after Mtb challenge largely corroborated the ELISpot data (*Figure S10C*).

i.v. BCG-elicited antigen-specific CD4 T cells in airways correlate with protection

In this study, we pre-specified a statistical analysis plan that included four immune features as primary potential correlates of protection: the number and frequency of mycobacterial-specific CD4 and CD8 T cells in airways (BAL). At the study end, we performed a logistic regression analysis (*Table S2*) using each of these four immunological parameters with protection (defined as <100 total thoracic Mtb CFU). Independent of i.v. BCG dose, the frequency and number of stimulated CD4 T cells producing any combination of IFN γ , IL-2, TNF, or IL-17

in the BAL were significant predictors of protection ($p = 0.0095$ and $p = 0.0074$). For each 1% increase in frequency or 10-fold increase in the number of antigen-specific CD4 T cells, the odds of protection increased by 27% (odds ratio of 1.2659) or 78-fold (odds ratio of 78.0348), respectively. Neither the frequency nor the number of cytokine-producing CD8 T cells significantly predicted protection when controlling for i.v. BCG dose.

Multivariate signatures more broadly correlate with i.v. BCG-elicited protection

Because we assessed a broad array of cellular and humoral immune features longitudinally throughout the vaccination phase (*Table S3*), we sought to evaluate the correlates of protection comprising multiple features using mathematical frameworks that accommodate the natural co-variation among them. Accordingly, we constructed computational models aiming to predict challenge outcomes from multi-feature signatures.

For each of the 18 protected macaques (<100 CFU) and 16 un-protected macaques (*Figure 6A*), we calculated the normalized area under the curve (nAUC) for each measured immune response feature as a simplification of the temporal dynamics after i.v. BCG (0 to 12 weeks), resulting in 68 nAUC measurements from BAL (*Figure S11A* and *Table S3*). Our first multivariate modeling approach evaluated the classification performance based on all measured BAL features concomitantly to provide a more integrative understanding of the i.v. BCG-elicited cellular and humoral responses beyond those revealed by univariate comparative statistics. Specifically, we used Least Absolute Shrinkage and Selection Operator (LASSO) feature selection²⁴ to select a minimal representative set of immune features from all available BAL measurements, followed by the classification of Partial Least Squares Discriminant Analysis (PLSDA) (*Figures 6B* and *6C*). LASSO/PLSDA analysis discriminated protected from non-protected animals using the i.v. BCG-induced immune response in BAL (*Figure 6B*). Four immune features from BAL were selected by LASSO as a minimal set that, together, predict protection: frequency of (PPD-specific) CD4 memory T cells producing IFN γ and TNF but not IL-2 or IL-17 ((L)%CD4:G+2-17-T+); frequency of CD4 memory T cells producing IL-17 and TNF but not IFN γ or IL-2 ((L)%CD4:G-2-17+T+); number of NK cells ((L)#NK); and the PPD-specific IgA titer ((L)IgA(PPD)) (*Figure 6C*). Model accuracy was significant ($p < 0.01$) relative to random permutation of outcome categories (*Figure 6G*), and the predictive sensitivity and specificity (confusion matrix) were strong (Matthews correlation coefficient [MCC] = 0.73; *Figure 6H*). Consistent with this minimal model, univariate analyses of these four selected features showed significant enrichment in protected compared with unprotected macaques (*Figure 6D*). To further probe the BAL immune profiles of i.v. BCG-induced longitudinal immune features between the protected and unprotected outcome groups, the mean percentile of each measurement was determined for both groups (*Figure 6E*). The polar area charts reveal that the protected group

(D and E) Heatmaps of LAM- (D) and PPD- (E) specific IgG1, IgA, and IgM antibody titers in the BAL after i.v. BCG. Titers (average of duplicate samples) are shown as the \log_2 fold change in Luminex MFI over the pre-vaccination (Pre) level.

(C and F) Correlation matrices including i.v. BCG dose and each antibody measurement in the plasma (C) and BAL (F). Positive correlations are red; negative correlations are blue. Values represent the Spearman's correlation coefficient. Ellipses have their eccentricity parametrically scaled to the strength of the relationship with statistical significance (unadjusted p value) indicated: < 0.05 (*), < 0.01 (**), < 0.001 (**), < 0.0001 (**), < 0.00001 (***).

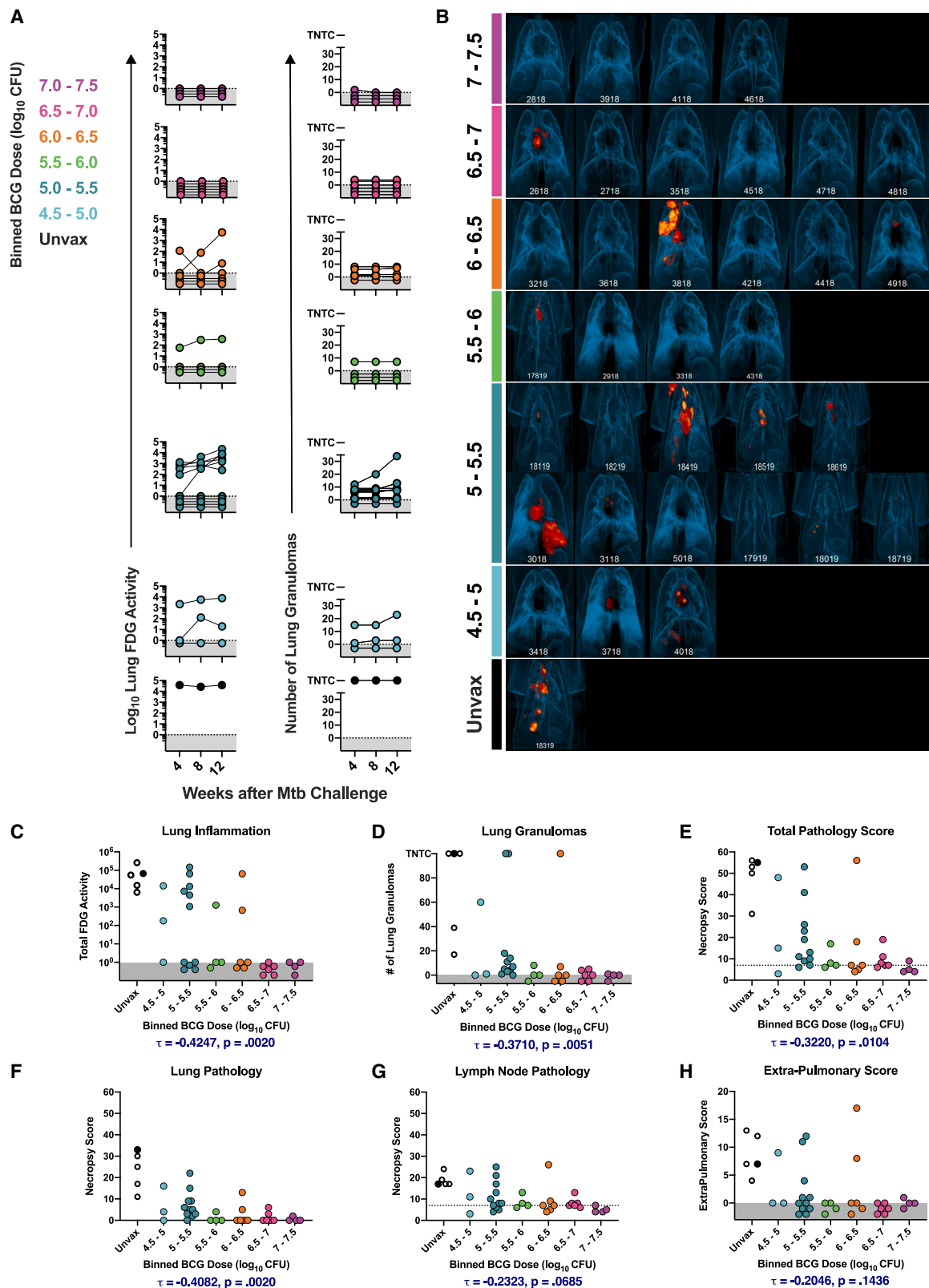


Figure 4. Outcomes of Mtb infection after varied i.v. BCG vaccination doses

(A) Lung inflammation (FDG activity) and number of lung granulomas over the course of infection measured by monthly PET CT scans for each macaque in each binned i.v. BCG dose group. Lines connect the same animal over time. TNTC; too numerous to count.

exhibited higher values of most feature categories from BAL including antibody titers, cell types present, and T cells with different expressed cytokines combinations. To gain insights into coordinated immune system processes represented by this model that differentiates protected versus unprotected groups, we built a correlation network connecting the LASSO-selected BAL features with other measured BAL features highly co-correlated with them (Figure 6F). This produced a substantial network comprising multiple additional features highly correlated with the four LASSO-selected features, e.g., including: CD4 T cells expressing a wider range of cytokine profiles (IFN γ , IL-2, TNF, IL-17, or IL-21); CD8 T cells expressing IFN γ , TNF, or IL-21; V γ 9 and MAIT cells; and a spectrum of antibody titers (IgG, IgA, and IgM) specific for LAM, WCL, or PPD. It should be noted that the pre-specified features (number [#] and frequency [%] of cytokine-producing CD4 T cells [CD4: AnyG2T17] in BAL [L]) shown as significant correlates in the logistic regression model described above (Table S2) appear in this correlation network.

To further substantiate these results, we incorporated data from an additional 10 rhesus macaques (n = 9 with Mtb CFU <100) that were vaccinated with high-dose i.v. BCG (>7.5 log₁₀ CFU) in a previous study⁷ and assessed the performance of our modeling approach using 54 immune measurements from BAL that overlapped between the two studies (Figure S12). Similar results were obtained, with the LASSO/PLSDA model obtaining the same four minimal features selected in the initial analysis above along with two additional: the numbers of CD4 and CD8 T cells expressing TNF and IFN γ ((L) #CD4:G+2-17-T+; (L)#CD8:G+2-17-T+)—both of which were found to be present in the foundational correlation network (Figure 6F). Although the foundational and extended (Figure S12E) correlation networks cannot easily be rigorously compared because the former includes features absent in the latter, we found 21 nodes in common (of 35 from the foundational network). Moreover, numerous other features, mainly immune cell types, are the same in both networks (although some are associated with cell numbers versus percentages). Thus, our multivariate approach is consistent across the combination of previous and new cohorts.

Since blood is the most accessible compartment from which to measure immune responses and define correlates of protection in human studies, we also evaluated longitudinal (0 to 24 weeks) immune data from the PBMC and plasma after i.v. BCG. First, we applied our LASSO/PLSDA procedure with correlation network analysis as above to 83 nAUC measurements derived from blood, including antibody titers and cytokines from plasma as well as flow cytometry data encompassing cellular composition and antigen-specific T cell responses (Figure S11). We again observed separation between the protected

and unprotected animals, albeit with significantly less specificity in blood compared with BAL (MCC = 0.68 for PBMC compared with 0.73 for BAL; p < 0.0001) (Figures S11B and S11H). In blood, separation was based on six selected features enriched in the protection group, namely plasma sCD40L and IL-8, cytokine-positive (Any) CD8 T cells also positive for granzyme B or CD107a, cytokine-producing CD4 effector memory T cells, and cytokine-positive V γ 9 $^{+}$ γ δ T cells positive for CD107a (Figure S11C). Again, these selected features demonstrated significant univariate differences between the two outcome groups (Figure S11D), and many measurements were enriched in the protected group based on the mean percentile quantitation (Figure S11E). Correlation network modeling revealed only two sparse networks (Figure S11F): a cluster of V γ 9 T cells expressing TNF or CD107a, and a network of CD4 T cells expressing CD154 and various cytokines (IFN γ , TNF, granzyme B). These data suggest that antigen-responsive V γ 9 T cells and CD4 T cells in the blood may be associated with the separation between protected and unprotected animals. Overall, a much less extensive set of immune system processes differentiating protection was found from blood measurements compared with those from the BAL.

Multivariate cellular immune signature after correction for i.v. BCG dose effects

The i.v. BCG vaccination dose correlated with the total Mtb CFU post-challenge (Figure 5A) as well as most humoral and cellular immune measurements in BAL and blood (Figure 7A). Thus, it was useful to include dose as an explicit covariate in our multivariate modeling. We employed a nested mixed linear modeling approach to evaluate immune response features with respect to association with protection status while controlling for the effects of i.v. BCG dose (as well as animal vaccination cohort). T values (normalized coefficients) of the protected group variable in the full model were calculated to quantify the magnitude of the i.v. BCG dose effect. Altogether, the measurements significantly associated with the protected group were defined as having a T value >2 and a two-sided LRT p value <0.05 in BAL (Figure 7B) and blood (Figure 7C). We observed that the only features that significantly differed between the two protection outcomes were enriched in the protected group and that there were a greater number of immune features from BAL compared with blood, which were enriched with protection (consistent with our PLSDA modeling results). In BAL (Figure 7B), three of the four LASSO-selected features (Figure 6C) remained significant after dose correction: the frequencies of CD4 T cells producing IFN γ and TNF or IL-17 and TNF ((L)%CD4:G+2-17-T+, (L)%CD4:G-2-17-T+) and the number of NK cells ((L)%NK). Of note, the immune features that were most strongly associated with

(B) Three-dimensional volume renderings of PET CT scans of the thoracic cavity of each macaque, arranged by dose group, just prior to necropsy. Areas of increasing orange/red coloring indicate FDG retention.

(C) Total lung FDG activity from pre-necropsy scan.

(D–H) Outcome data from necropsy: number of lung granulomas found at necropsy (D); total gross pathology score (E); pathology scores for lung (F), lymph node (G), and extrapulmonary tissues (H). Dashed line in (E) and (G) is assumed normal pathology score accounting for variability in thoracic lymph node size in healthy rhesus macaques. Symbols represent individual macaques. Data points within gray areas are zero. Open black symbols indicate unvaccinated (Unvax) historical controls.⁷ TNTC; too numerous to count. Nonparametric bivariate correlations between outcomes and dose shown with Kendall's τ and corresponding p value (blue).

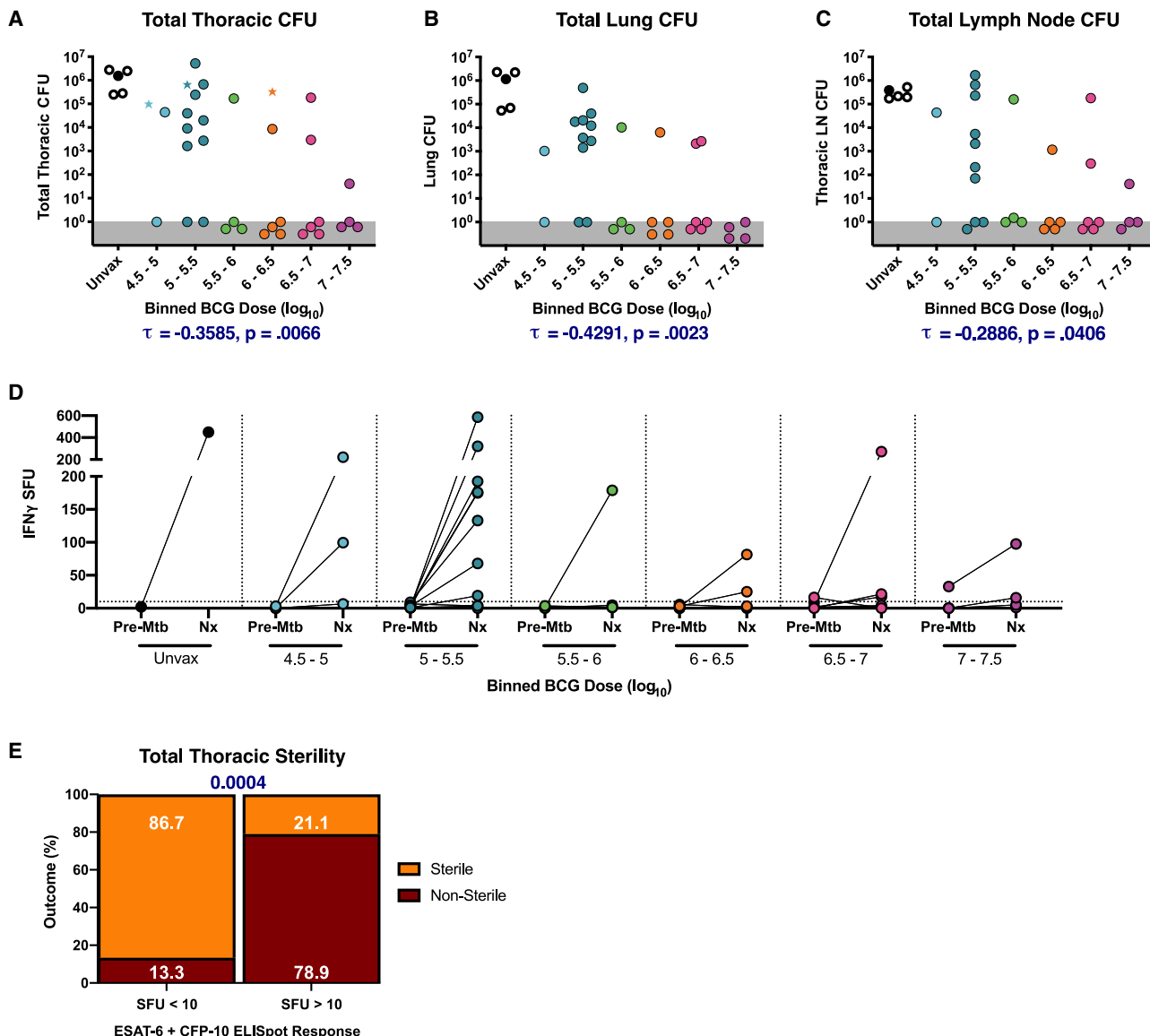


Figure 5. Mtb bacterial burdens after infection of i.v. BCG-vaccinated macaques

(A-C) Mtb bacterial burden (colony forming units; CFU) from the thoracic cavity of rhesus macaques necropsied 12 weeks post-challenge; total thoracic (A), lungs (B), or thoracic lymph nodes (C). Open symbols represent historical unvaccinated controls⁷ and star-shaped symbols indicate predicted total thoracic CFU based on total thoracic lung inflammation from PET CT.²³ Data points within gray areas are zero. Sterility was defined 0 thoracic CFU, whereas protection was defined as <100 thoracic CFU. Nonparametric bivariate correlations between outcomes and dose (Kendall's τ and corresponding p value).

(D) PBMC IFN γ ELISpots to antigens present in Mtb but not BCG (ESAT-6 and CFP-10) prior to Mtb challenge (Pre-Mtb) and at necropsy (Nx). Lines show individual macaques over time for each binned dose group. Dashed horizontal line represents the cut-off below which at least 95% of uninfected animals fall. See also Figure S10A.

(E) Percentage of sterile or non-sterile macaques either positive or negative by ELISPOT. Fisher's exact test p value (two-sided).

protection in the BAL were the number of CD4 T cells producing any combination of IFN γ , IL-2, TNF, or IL17 ($(L)\#CD4:A\#nyG2T17$) and the number of CD4 T cells producing IFN γ with or without other cytokines ($(L)\#CD4:G$). In blood (Figure 7C), only one of the six LASSO-selected features (Figure S11C) remained significant after dose correction: plasma levels of sCD40L. These findings confirm that our PLSDA models are not exclusively dominated by i.v. BCG dose and that the frequency and number of mycobacterial-specific

CD4 T cells in the BAL are significant correlates of protection, independent of BCG dose.

DISCUSSION

Defining vaccine-elicited immune correlates of protection will facilitate TB vaccine development by informing vaccine trial design and providing a rationale for selecting vaccine formulations or regimens that elicit a protective response. Additionally,

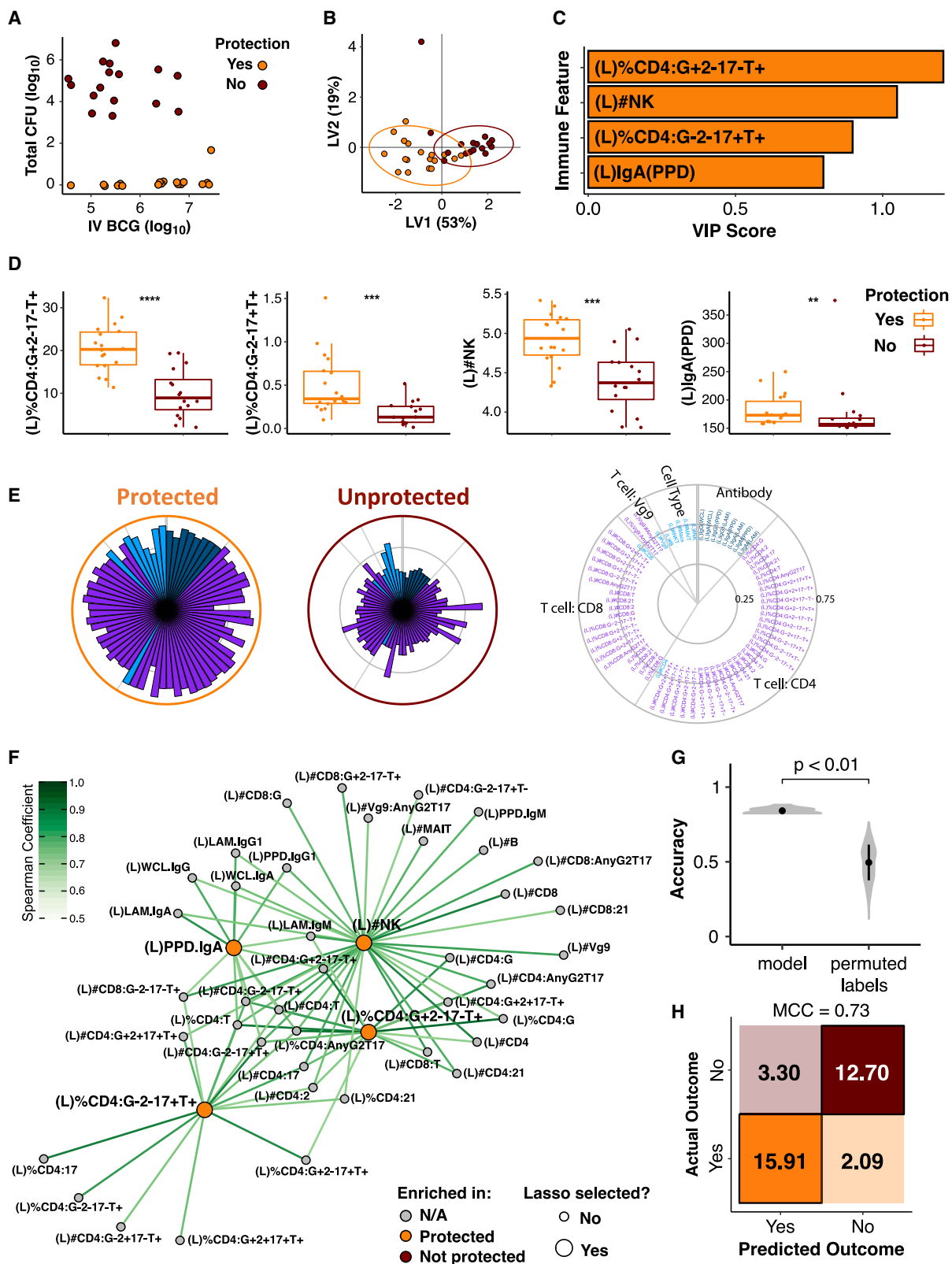


Figure 6. Selected immune parameters from BAL distinguish protection in i.v. BCG-vaccinated macaques

(A–D) PLSDA following LASSO was applied to identify immune features in BAL (L, lung) that distinguish protected and unprotected animals. (A) Animals with <100 total thoracic Mtb CFU (n = 18) were defined as protected (yes, orange). (B) The PLSDA scores plot shows the degree of discrimination between protected and

(legend continued on next page)

correlates of protection can guide a deeper investigation of mechanisms of protection. Nonhuman primates are a predictive model for evaluating vaccines against various infectious diseases as they recapitulate the innate and adaptive immune features elicited in humans following vaccination. Moreover, the model allows for longitudinal sampling of BAL and blood, providing data on whether tissue- and blood-derived correlates might be distinct. The finding that high-dose i.v. BCG vaccination can prevent TB infection in macaques makes this a valuable pre-clinical model for defining correlates and mechanisms of protection.

A unique feature of this study is that all animals received the same vaccine (i.v. BCG), whereas the dose was varied to achieve a range of immune responses and disparate outcomes. We observed 53% overall protection (18 of 34), with 17 animals showing sterile protection. Collectively, we assessed many immune variables, including innate, humoral, and cellular measures in blood and BAL to capture a broad array of potential correlates of protection and then employed an integrative multivariate modeling approach that incorporates the observed co-variation among immune features to produce latent variables that correlate with protection. In our statistical analysis plan, we pre-specified four immune measurements as primary correlates and found that two, the frequency and number of antigen-specific CD4 T cells in the BAL, were significant correlates of protection, independent of the BCG dose. Post-hoc multivariate analysis of blood- and BAL-derived immune features substantiated the correlation of Th1/Th17 cytokine-producing CD4 T cells in the BAL and identified NK cells and other CD8 α -expressing cells in BAL in an immune network of protection against TB.

Recently, Dijkman et al. showed protection against repeated limiting dose Mtb challenge in macaques that were vaccinated with BCG directly into the lung by bronchoscopic instillation.⁸ Mucosally vaccinated animals generated robust CD4 T cell responses in BAL, with polyfunctional Th17 cells correlating with protection. In addition, IgA titers in the BAL fluid, and IL-10 production from restimulated BAL cells also correlated with protection. Notably, the identified correlates were found from BAL and not in blood measurements. An earlier study by Sharpe et al., in which NHP were vaccinated with BCG ID, also identified a Th1/Th17 signature in the blood of vaccinated animals.¹⁷ Further, in a latency model, CD4 Th1 cells expressing IL-17 and IL-10 were present at higher levels in granulomas that controlled infection.¹² Finally, in a rhesus latency model using the low virulence Mtb strain (CDC1551) for infection, mucosal CXCR3 $^+$ CCR6 $^+$ CD4 Th1/Th17 cells appeared early in the BAL, but not blood, and corresponded to asymptomatic

infection and lower Mtb burdens in the lung.¹⁶ Collectively, these macaque studies with BCG vaccination or Mtb infection highlight the importance of measuring airway responses to define correlates of protection. In addition, they provide mounting evidence pointing to lung-localized adaptive immunity as a causal mediator of protection.

Here, we applied LASSO to our large array of immune measurements to select the most parsimonious set of variables. For BAL measurements, a resulting minimal model exhibiting statistical significance and strong predictive capability comprised only four features: frequency of CD4 T cells producing IFN γ and TNF but not IL-2 or IL-17; frequency of CD4 T cells producing IL-17 and TNF but not IFN γ or IL-2; the absolute number of NK cells; and the PPD-specific IgA titer. The first three of these remained significant after employing a mixed linear model that accounted for strong i.v. BCG vaccine dose effects. An analogous multivariate model based on immune features measured in blood was far less effective at discriminating protection.

We next sought the interpretation of the broader immune processes represented by this multivariate signature by constructing a correlation network model incorporating a wider set of features that strongly co-varied with the minimal set. Although LASSO-selected BAL CD4 T cells that produced either IFN γ and TNF, or IL-17 and TNF, for the minimal PLSDA model, CD4 T cells that produced most other combinations of IFN γ , IL-2, TNF, and IL-17 were highly co-correlated, indicating that their capability to predict protection was nearly as strong as the LASSO-selected features themselves. Thus, discrimination between protected and unprotected animals does not appear to be exclusively limited to a specific Th1 or Th17 cytokine combination but rather a coordinated response involving diverse T cell functions. Our results here differ from Dijkman et al., who found that the quadruple-positive (IFN γ $^+$ IL-2 $^+$ TNF $^+$ IL-17 $^+$) subset of BCG-specific BAL CD4 T cells correlated with protection, along with IgA in the airway and IL-10 from restimulated BAL cells.⁸ In our study, IL-10 was not measured from BAL cells, and plasma levels of IL-10 after i.v. BCG did not correlate with protection; furthermore, although we observed an initial correlation between antibody titers and protection, these measures were not significant following dose correction. Nevertheless, the finding that antigen-specific CD4 Th1/Th17 cells in the lung (site of infection), but not the blood, associate with protection is consistent across many prior studies.

Notably, the number of NK cells in BAL was a selected minimal feature for predicting protection and remained significant after correcting for vaccine dose. An NK cell blood transcriptional

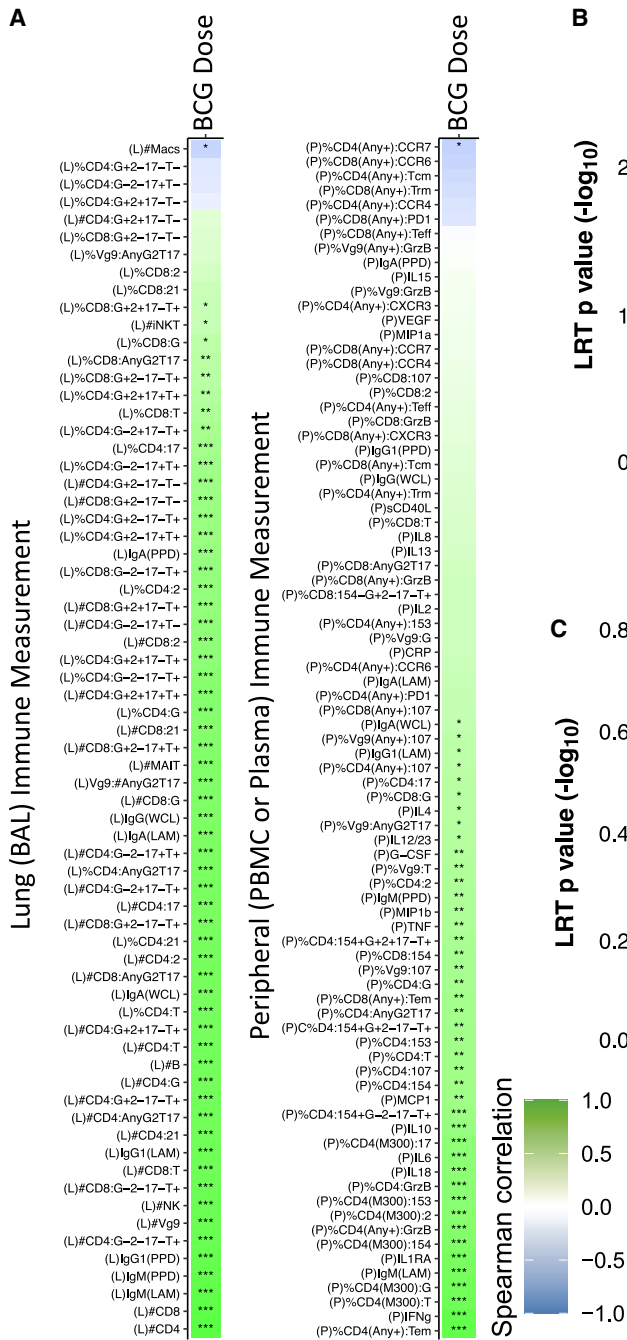
unprotected animals following LASSO feature selection; symbols represent individual macaques, and ellipses indicate 95% confidence regions assuming a multivariate t distribution. (C) VIP (variable importance in projection) scores of the 4 LASSO-selected features that together discriminate protection. (D) Univariate box plots show the distribution of each selected feature in protected or unprotected animals. Boxes show interquartile range (IQR) with median (line) and whiskers (1.5*IQR). * $p < 0.05$, ** $p < 0.01$, *** $p < 0.001$, **** $p < 0.0001$ (Wilcoxon).

(E) Polar plots depict the mean percentile of each measurement across the protected and the unprotected groups. Wedge distance from center depicts the mean percentile from 0 to 0.75 with a step of 0.25.

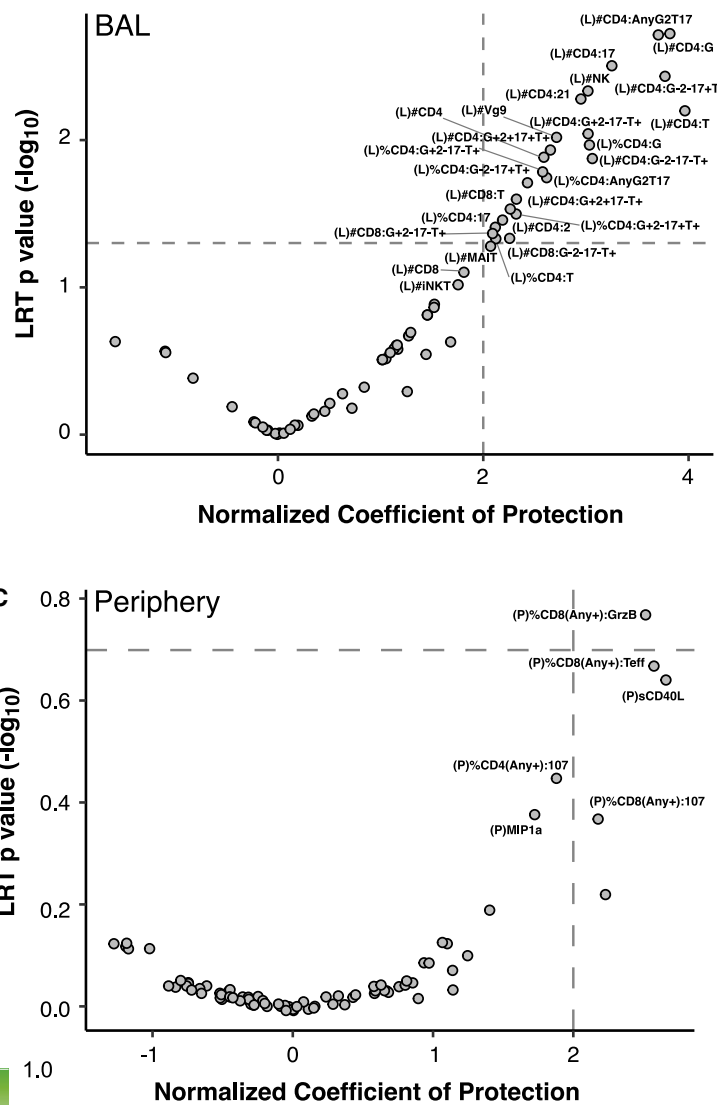
(F) A correlation network shows the immune features (gray nodes) that are significantly co-correlated ($p < 0.05$ after Benjamini-Hochberg correction; Spearman's > 0.7) with model-selected features (orange nodes) from (C). See also Table S3.

(G and H) Model performance and robustness are validated with permutation testing and confusion matrix. (G) The violin plot shows the distributions of repeated classification accuracy testing using label permutation (two-sided p value). Black circles show median accuracy and black lines represent one SD. (H) Average confusion matrix of the PLSDA model with Matthews correlation coefficient (MCC).

A



B



C

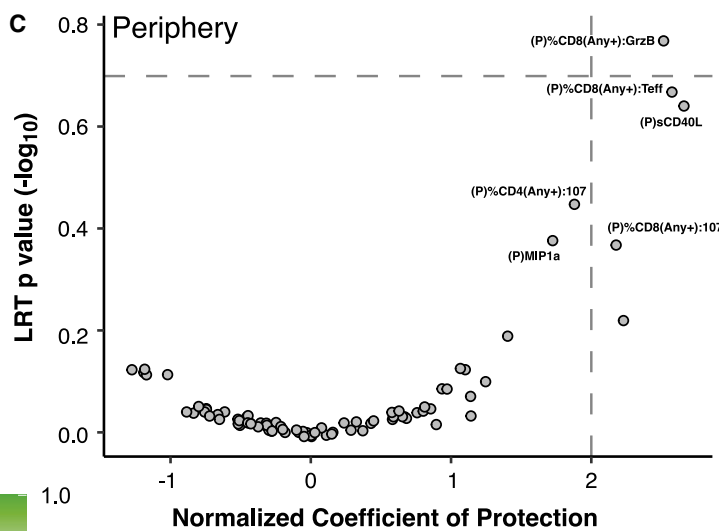


Figure 7. Immune features in BAL and blood associate with protection after controlling for i.v. BCG dose

(A) Spearman's correlation between each immune measurement in BAL (L, lung) or blood (P, PBMC or plasma) and i.v. BCG dose. Adjusted p values after Benjamini-Hochberg correction (* p < 0.05, ** p < 0.01, *** p < 0.001, **** p < 0.0001).

(B and C) A nested mixed linear model was created for each immune measurement with and without a variable accounting for the animals' protection group. The volcano plot shows the T value (normalized coefficient) of protection incorporated in the mixed linear model (x axis) vs the p value of the likelihood ratio test (LRT) for the model fit difference between the two nested models (y axis) using BAL- (B) and blood- (C) derived measurements. Positive T values represent features enriched in the protected group. See also Table S3.

signature was observed 3 weeks after aerosol vaccination with an Mtb sigH mutant (but not after aerosol BCG), a regimen that protected rhesus macaques from CDC1551 Mtb challenge.²⁵ NK cells were also reported to accumulate in the lungs of latent

versus active CDC1551-infected rhesus macaques.²⁶ In humans, intradermal BCG-re-vaccination boosted IFN γ -producing mycobacteria-responsive NK cell responses for at least 1 year.²⁷ It should be noted that our network analysis shows that the

number of NK cells in BAL correlated with several other cell subsets that also express CD8 α (e.g., CD8 T cells, V γ 9 $^+$ γ δ T cells, and MAIT cells). Here, we did not evaluate cytokine or cytolytic function in NK cells; however, we speculate that these “innate” T or NK cells might contribute to i.v. BCG-elicited protection through direct effector function or by promoting adaptive T cell responses, as has been shown in models of TB and malaria.^{28,29}

Although our univariate analysis did not validate the number or frequency of antigen-specific CD8 T cells in the BAL as a correlate of protection from infection, there is increasing evidence that the cytotoxic functionality of CD8 T cells may play a role in controlling Mtb.¹⁸

Finally, in a separate analysis of the blood transcriptomics from these animals, Liu et al. (*Cell Reports Medicine*, accepted for upcoming publication) identify an innate signature at day 2 following i.v. BCG administration that predicts the subsequent adaptive BAL responses associated with protection described here—and, in fact, show that this signature predicts protection with a high degree of accuracy. These analyses suggest that early immune events following vaccination with i.v. BCG may be a more facile approach for predicting protection.

In conclusion, we demonstrate that prevention Mtb infection in a highly stringent rhesus macaque model can be achieved by immunization with i.v. BCG across a wide range of doses and that Th1/Th17 responses in the airway predict protective outcome. This suggests that early-phase clinical trials will gain considerable insight into immune correlates by assessing BAL, in addition to blood, in a subset of individuals. Ongoing studies depleting CD4 or CD8 T cells from i.v. BCG-immunized macaques prior to the challenge will further define mechanistic correlates of protection. These data provide a roadmap for developing a highly successful vaccine against TB that encompasses having a sufficient magnitude and breadth of Th1/Th17 and possibly CD8 T cell responses, and importantly, considering how changing the route of vaccination can lead to the generation of a high frequency of antigen-specific T cells at the site of infection.

STAR★METHODS

Detailed methods are provided in the online version of this paper and include the following:

- **KEY RESOURCES TABLE**
- **RESOURCE AVAILABILITY**
 - Lead contact
 - Materials availability
 - Data code and availability
- **EXPERIMENTAL MODEL AND SUBJECT DETAILS**
 - Animals
- **METHOD DETAILS**
 - Study design
 - BCG vaccination
 - Mtb challenge
 - Sample processing
 - Multiparameter flow cytometry
 - ELISpot and milliplex assays
 - Antibody levels
 - PET CT scans and analysis
 - Necropsy, pathology scoring, and Mtb burden

● QUANTIFICATION AND STATISTICAL ANALYSIS

- Data preprocessing
- Quantification and statistics
- Polar plot
- Multivariate modeling
- Correlation networks
- Linear mixed modeling

SUPPLEMENTAL INFORMATION

Supplemental information can be found online at <https://doi.org/10.1016/j.chom.2023.05.006>.

ACKNOWLEDGMENTS

This work was supported by the Intramural Research Program of the VRC; NIH contract #75N93019C00071 (S.M.F., J.L.F., and D.A.L.); NIH R01 award: AI152158 (D.A.L.); NIH F31 award: AI150171-01 (E.B.I., S.M.F., and G.A.); BMGF INV-020435 (J.L.F.). We thank veterinary and research technicians (D. Fillmore, C. Ameel, A. Myers, and C. Bigbee), and imaging personnel (LJ Frye) at the University of Pittsburgh and members of the VRC Translational Research Program (R. Woodward and J.P. Todd), as well as BioQual, Inc for animal care. We thank the VRC Flow cytometry Core for support and members of the Flynn and Seder laboratories for discussions.

AUTHOR CONTRIBUTIONS

Conceptualization, P.A.D., J.L.F., R.A.S., P.M., and M.R.; data curation, P.A.D., J.J.Z., C.W., E.B.I., G.A., D.A.L., P.M., and M.R.; formal analysis, P.A.D., J.J.Z., C.W., E.B.I., G.A., D.A.L., P.M., and M.R.; funding acquisition, G.A., S.M.F., D.A.L., J.L.F., R.A.S., and M.R.; investigation, P.A.D., J.J.Z., E.B.I., A.N.B., M.A.R., S.P., J.A.H., M.K., A.G.W., H.J.B., L.J.F., J.T., K.K., P.L.L., E.K., and C.A.S.; methodology, P.A.D., C.W., E.B.I., P.L.L., C.A.S., and G.A.; project administration, P.A.D., C.A.S.; supervision, G.A., S.M.F., D.A.L., J.L.F., R.A.S., and M.R.; visualization, P.A.D., J.J.Z., C.W., E.B.I., P.M., and M.R.; writing—original draft, P.A.D., J.J.Z., C.W., E.B.I., J.L.F., R.A.S., D.A.L., P.M., and M.R.; writing—review and editing, all authors.

DECLARATION OF INTERESTS

The authors declare no competing interests.

INCLUSION AND DIVERSITY

We support inclusive, diverse, and equitable conduct of research.

Received: November 4, 2022

Revised: March 9, 2023

Accepted: May 9, 2023

Published: June 1, 2023

REFERENCES

1. Martinez, L., Cords, O., Liu, Q., Acuna-Villaorduna, C., Bonnet, M., Fox, G.J., Carvalho, A.C.C., Chan, P.-C., Croda, J., Hill, P.C., et al. (2022). Infant BCG vaccination and risk of pulmonary and extrapulmonary tuberculosis throughout the life course: a systematic review and individual participant data meta-analysis. *Lancet Glob. Health* 10, e1307–e1316. [https://doi.org/10.1016/S2214-109X\(22\)00283-2](https://doi.org/10.1016/S2214-109X(22)00283-2).
2. Carpenter, S.M., and Lu, L.L. (2022). Leveraging antibody, B cell and Fc receptor interactions to understand heterogeneous immune responses in tuberculosis. *Front. Immunol.* 13, 830482. <https://doi.org/10.3389/fimmu.2022.830482>.
3. Sia, J.K., and Rengarajan, J. (2019). Immunology of *Mycobacterium tuberculosis* infections. *Microbiol. Spectr.* 7. <https://doi.org/10.1128/microbiol-spec.GPP3-0022-2018>.

4. Bellamy, R. (2003). Susceptibility to mycobacterial infections: the importance of host genetics. *Genes Immun.* 4, 4–11. <https://doi.org/10.1038/sj.gene.6363915>.
5. Godfrey, M.S., and Friedman, L.N. (2019). Tuberculosis and biologic therapies: anti-tumor necrosis factor-alpha and beyond. *Clin. Chest Med.* 40, 721–739. <https://doi.org/10.1016/j.ccm.2019.07.003>.
6. Larsen, S.E., Williams, B.D., Rais, M., Coler, R.N., and Baldwin, S.L. (2022). It takes a village: the multifaceted immune response to *Mycobacterium tuberculosis* infection and vaccine-induced immunity. *Front. Immunol.* 13, 840225. <https://doi.org/10.3389/fimmu.2022.840225>.
7. Darrah, P.A., Zeppa, J.J., Maiello, P., Hackney, J.A., Wadsworth, M.H., 2nd, Hughes, T.K., Pokkali, S., Swanson, P.A., 2nd, Grant, N.L., Rodgers, M.A., et al. (2020). Prevention of tuberculosis in macaques after intravenous BCG immunization. *Nature* 577, 95–102. <https://doi.org/10.1038/s41586-019-1817-8>.
8. Dijkman, K., Sombroek, C.C., Vervenne, R.A.W., Hofman, S.O., Boot, C., Remarque, E.J., Kocken, C.H.M., Ottenhoff, T.H.M., Kondova, I., Khayum, M.A., et al. (2019). Prevention of tuberculosis infection and disease by local BCG in repeatedly exposed rhesus macaques. *Nat. Med.* 25, 255–262. <https://doi.org/10.1038/s41591-018-0319-9>.
9. Hansen, S.G., Zak, D.E., Xu, G., Ford, J.C., Marshall, E.E., Malouli, D., Gilbride, R.M., Hughes, C.M., Ventura, A.B., Ainslie, E., et al. (2018). Prevention of tuberculosis in rhesus macaques by a cytomegalovirus-based vaccine. *Nat. Med.* 24, 130–143. <https://doi.org/10.1038/nm.4473>.
10. Sharpe, S., White, A., Sarfas, C., Sibley, L., Gleeson, F., McIntyre, A., Basaraba, R., Clark, S., Hall, G., Rayner, E., et al. (2016). Alternative BCG delivery strategies improve protection against *Mycobacterium tuberculosis* in non-human primates: protection associated with mycobacterial antigen-specific CD4 effector memory T-cell populations. *Tuberculosis (Edinb)* 101, 174–190. <https://doi.org/10.1016/j.tube.2016.09.004>.
11. Irvine, E.B., O’Neil, A., Darrah, P.A., Shin, S., Choudhary, A., Li, W., Honnen, W., Mehra, S., Kaushal, D., Gideon, H.P., et al. (2021). Robust IgM responses following intravenous vaccination with bacille calmette-guerin associate with prevention of *Mycobacterium tuberculosis* infection in macaques. *Nat. Immunol.* 22, 1515–1523. <https://doi.org/10.1038/s41590-021-01066-1>.
12. Gideon, H.P., Phuah, J., Myers, A.J., Bryson, B.D., Rodgers, M.A., Coleman, M.T., Maiello, P., Rutledge, T., Marino, S., Fortune, S.M., et al. (2015). Variability in tuberculosis granuloma T cell responses exists, but a balance of pro- and anti-inflammatory cytokines is associated with sterilization. *PLoS Pathog.* 11, e1004603. <https://doi.org/10.1371/journal.ppat.1004603>.
13. Gopal, R., Rangel-Moreno, J., Slight, S., Lin, Y., Nawar, H.F., Fallert Junecko, B.A., Reinhart, T.A., Kolls, J., Randall, T.D., Connell, T.D., and Khader, S.A. (2013). Interleukin-17-dependent CXCL13 mediates mucosal vaccine-induced immunity against tuberculosis. *Mucosal Immunol.* 6, 972–984. <https://doi.org/10.1038/mi.2012.135>.
14. Khader, S.A., Bell, G.K., Pearl, J.E., Fountain, J.J., Rangel-Moreno, J., Cilley, G.E., Shen, F., Eaton, S.M., Gaffen, S.L., Swain, S.L., et al. (2007). IL-23 and IL-17 in the establishment of protective pulmonary CD4+ T cell responses after vaccination and during *Mycobacterium tuberculosis* challenge. *Nat. Immunol.* 8, 369–377. <https://doi.org/10.1038/ni1449>.
15. Lindestam Arlehamn, C.S., Gerasimova, A., Mele, F., Henderson, R., Swann, J., Greenbaum, J.A., Kim, Y., Sidney, J., James, E.A., Taplitz, R., et al. (2013). Memory T cells in latent *Mycobacterium tuberculosis* infection are directed against three antigenic islands and largely contained in a CXCR3+CCR6+ Th1 subset. *PLoS Pathog.* 9, e1003130. <https://doi.org/10.1371/journal.ppat.1003130>.
16. Shanmugasundaram, U., Bucsan, A.N., Ganatra, S.R., Ibegbu, C., Quezada, M., Blair, R.V., Alvarez, X., Veliu, V., Kaushal, D., and Rengarajan, J. (2020). Pulmonary *Mycobacterium tuberculosis* control associates with CXCR3- and CCR6-expressing antigen-specific Th1 and Th17 cell recruitment. *JCI Insight* 5, e137858. <https://doi.org/10.1172/jci.insight.137858>.
17. Wareham, A.S., Tree, J.A., Marsh, P.D., Butcher, P.D., Dennis, M., and Sharpe, S.A. (2014). Evidence for a role for interleukin-17, Th17 cells and iron homeostasis in protective immunity against tuberculosis in cynomolgus macaques. *PLoS One* 9, e88149. <https://doi.org/10.1371/journal.pone.0088149>.
18. Gideon, H.P., Hughes, T.K., Tzouanas, C.N., Wadsworth, M.H., 2nd, Tu, A.A., Gierahn, T.M., Peters, J.M., Hopkins, F.F., Wei, J.R., Kummerlowe, C., et al. (2022). Multimodal profiling of lung granulomas in macaques reveals cellular correlates of tuberculosis control. *Immunity* 55, 827–846.e10. <https://doi.org/10.1016/j.jimmuni.2022.04.004>.
19. Ogongo, P., Tezera, L.B., Arda, N., Nhamoyebonde, S., Ramsuran, D., Singh, A., Ng’oep, A., Karim, F., Naidoo, T., Khan, K., et al. (2021). Tissue-resident-like CD4+ T cells secreting IL-17 control *Mycobacterium tuberculosis* in the human lung. *J. Clin. Invest.* 131, e142014. <https://doi.org/10.1172/JCI142014>.
20. Scriba, T.J., Penn-Nicholson, A., Shankar, S., Hraha, T., Thompson, E.G., Sterling, D., Nemes, E., Darboe, F., Suliman, S., Amon, L.M., et al. (2017). Sequential inflammatory processes define human progression from *M. tuberculosis* infection to tuberculosis disease. *PLoS Pathog.* 13, e1006687. <https://doi.org/10.1371/journal.ppat.1006687>.
21. Brown, E.P., Licht, A.F., Dugast, A.S., Choi, I., Bailey-Kellogg, C., Alter, G., and Ackerman, M.E. (2012). High-throughput, multiplexed IgG subclassing of antigen-specific antibodies from clinical samples. *J. Immunol. Methods* 386, 117–123. <https://doi.org/10.1016/j.jim.2012.09.007>.
22. Coleman, M.T., Maiello, P., Tomko, J., Frye, L.J., Fillmore, D., Janssen, C., Klein, E., and Lin, P.L. (2014). Early Changes by (18)fluorodeoxyglucose positron emission tomography coregistered with computed tomography predict outcome after *Mycobacterium tuberculosis* infection in cynomolgus macaques. *Infect. Immun.* 82, 2400–2404. <https://doi.org/10.1128/IAI.01599-13>.
23. Maiello, P., DiFazio, R.M., Cadena, A.M., Rodgers, M.A., Lin, P.L., Scanga, C.A., and Flynn, J.L. (2018). Rhesus macaques are more susceptible to progressive tuberculosis than cynomolgus macaques: a quantitative comparison. *Infect. Immun.* 86, e00505–e00517. <https://doi.org/10.1128/IAI.00505-17>.
24. Bartsch, Y.C., Wang, C., Zohar, T., Fischinger, S., Atyeo, C., Burke, J.S., Kang, J., Edlow, A.G., Fasano, A., Baden, L.R., et al. (2021). Humoral signatures of protective and pathological SARS-CoV-2 infection in children. *Nat. Med.* 27, 454–462. <https://doi.org/10.1038/s41591-021-01263-3>.
25. Kaushal, D., Foreman, T.W., Gautam, U.S., Alvarez, X., Adekambi, T., Rangel-Moreno, J., Golden, N.A., Johnson, A.M., Phillips, B.L., Ahsan, M.H., et al. (2015). Mucosal vaccination with attenuated *Mycobacterium tuberculosis* induces strong central memory responses and protects against tuberculosis. *Nat. Commun.* 6, 8533. <https://doi.org/10.1038/ncomms9533>.
26. Esaulova, E., Das, S., Singh, D.K., Chorenio-Parra, J.A., Swain, A., Arthur, L., Rangel-Moreno, J., Ahmed, M., Singh, B., Gupta, A., et al. (2021). The immune landscape in tuberculosis reveals populations linked to disease and latency. *Cell Host Microbe* 29, 165–178.e8. <https://doi.org/10.1016/j.chom.2020.11.013>.
27. Suliman, S., Geldenhuys, H., Johnson, J.L., Hughes, J.E., Smit, E., Murphy, M., Toefy, A., Lerumo, L., Hopley, C., Pienaar, B., et al. (2016). *Bacillus Calmette-Guerin* (BCG) revaccination of adults with latent *Mycobacterium tuberculosis* infection induces long-lived BCG-reactive NK cell responses. *J. Immunol.* 197, 1100–1110. <https://doi.org/10.4049/jimmunol.1501996>.
28. Ruibal, P., Voogd, L., Joosten, S.A., and Ottenhoff, T.H.M. (2021). The role of donor-unrestricted T-cells, innate lymphoid cells, and NK cells in anti-mycobacterial immunity. *Immunol. Rev.* 301, 30–47. <https://doi.org/10.1111/imr.12948>.
29. Zaidi, I., Diallo, H., Conteh, S., Robbins, Y., Kolasny, J., Orr-Gonzalez, S., Carter, D., Butler, B., Lambert, L., Brickley, E., et al. (2017). $\gamma\delta$ T cells are required for the induction of sterile immunity during irradiated sporozoite

- vaccinations. *J. Immunol.* 199, 3781–3788. <https://doi.org/10.4049/jimmunol.1700314>.
30. Capuano, S.V., 3rd, Croix, D.A., Pawar, S., Zinovik, A., Myers, A., Lin, P.L., Bissel, S., Fuhrman, C., Klein, E., and Flynn, J.L. (2003). Experimental *Mycobacterium tuberculosis* infection of cynomolgus macaques closely resembles the various manifestations of human *M. tuberculosis* infection. *Infect. Immun.* 71, 5831–5844. <https://doi.org/10.1128/IAI.71.10.5831-5844.2003>.
31. Lindestam Arlehamn, C.S., McKinney, D.M., Carpenter, C., Paul, S., Rozot, V., Makgolho, E., Gregg, Y., van Rooyen, M., Ernst, J.D., Hatherill, M., et al. (2016). A quantitative analysis of complexity of human pathogen-specific CD4 T cell responses in healthy *M. tuberculosis* infected South Africans. *PLoS Pathog.* 12, e1005760. <https://doi.org/10.1371/journal.ppat.1005760>.
32. Corbett, A.J., Eckle, S.B., Birkinshaw, R.W., Liu, L., Patel, O., Mahony, J., Chen, Z., Reantragoon, R., Meehan, B., Cao, H., et al. (2014). T-cell activation by transitory neo-antigens derived from distinct microbial pathways. *Nature* 509, 361–365. <https://doi.org/10.1038/nature13160>.
33. Schlottmann, S.A., Jain, N., Chirmule, N., and Esser, M.T. (2006). A novel chemistry for conjugating pneumococcal polysaccharides to Luminex microspheres. *J. Immunol. Methods* 309, 75–85. <https://doi.org/10.1016/j.jim.2005.11.019>.
34. White, A.G., Maiello, P., Coleman, M.T., Tomko, J.A., Frye, L.J., Scanga, C.A., Lin, P.L., and Flynn, J.L. (2017). Analysis of 18FDG PET/CT imaging as a tool for studying *Mycobacterium tuberculosis* infection and treatment in non-human primates. *J. Vis. Exp.* 127, 56375. <https://doi.org/10.3791/56375>.

STAR★METHODS

KEY RESOURCES TABLE

REAGENT or RESOURCE	SOURCE	IDENTIFIER
Antibodies		
BV510 Mouse anti-NHP CD45 (clone D058-1283)	BD Biosciences	Cat# 563530; RRID: AB_2738262
BV650 Mouse anti-human CD3 (clone SP34-2)	BD Biosciences	Cat# 563916; RRID: AB_2738486
BUV395 Mouse anti-human CD8 (clone RPA-T8)	BD Biosciences	Cat# 563795; RRID: AB_2722501
TCR gamma/delta monoclonal antibody, PE (clone 5A6.E9)	Thermo Fisher Scientific	Cat# MHGD04; RRID: AB_10374518
TCR V gamma 9 monoclonal antibody, custom Alexa Fluor 680 custom-conjugated (clone 7A5)	Thermo Fisher Scientific	Cat# TCR1720; RRID: AB_417089
Mouse anti-human CD69, ECD (clone TP1.55.3)	Beckman Coulter	Cat# 6607110; RRID: AB_1575978
Mouse anti-human CD159a (NKG2A), APC (clone Z199)	Beckman Coulter	Cat# A60797; RRID: AB_10643105
Brilliant Violet 570 anti-human CD20 (clone 2H7)	BioLegend	Cat# 302332; RRID: AB_2563805
Brilliant Violet 605 anti-human CD11b Antibody (clone ICRF44)	BioLegend	Cat# 301332; RRID: AB_2562021
APC/Cyanine7 anti-human CD163 (clone GH1-61)	BioLegend	Cat# 333622; RRID: AB_2563612
BUV805 Mouse anti-human CD8 (clone SK1)	BD Biosciences	Cat# 612889; RRID: AB_2833078
PE-Cy5 Mouse anti-human CD28 (clone CD28.2)	BD Biosciences	Cat# 555730; RRID: AB_396073
Brilliant Violet 711 anti-human CD183 (CXCR3) (clone G025H7)	BioLegend	Cat# 353732; RRID: AB_2563533
BUV737 Mouse anti-human CD196 (CCR6) (clone 11A9)	BD Biosciences	Cat# 612780; RRID: AB_2870109
APC-Cy7 Mouse anti-human CD3 (clone SP34-2)	BD Biosciences	Cat# 557757; RRID: AB_396863
APC Mouse anti-human IFN- γ (clone B27)	BD Biosciences	Cat# 554702; RRID: AB_398580
BV750 Rat anti-human IL-2 (clone MQ1-17H12)	BD Biosciences	Cat# 566361; RRID: AB_2739710
BV650 Mouse anti-human TNF (clone Mab11)	BD Biosciences	Cat# 563418; RRID: AB_2738194
Brilliant Violet 711 anti-human CD183 (CXCR3) (clone BL168)	BioLegend	Cat# 512324; RRID: AB_2563886
BUV496 Mouse anti-human CD4 (clone L200)	BD Biosciences	Cat# 750591; RRID: AB_2874725
Mouse anti-human TCR V gamma 9, FITC (clone 7A5)	Thermo Fisher Scientific	Cat# TCR2720; RRID: AB_417094
Alexa Fluor 700 Mouse anti-human CD197 (CCR7) (clone 150503)	BD Biosciences	Cat# 561143; RRID: AB_10562031
Brilliant Violet 605 anti-human CD183 (CXCR3) (clone G025H7)	BD Biosciences	Cat# 612780; RRID: AB_2870109
Mouse anti-human CD185 (CXCR5), Super Bright 600 (clone MU5UBEE)	Thermo Fisher Scientific	Cat# 63-9185-42; RRID: AB_2724065
Mouse anti-human CD279 (PD-1) BB660 custom-conjugated (clone EH12.1)	BD Biosciences	N/A

(Continued on next page)

Continued

REAGENT or RESOURCE	SOURCE	IDENTIFIER
R718 Armenian hamster anti-ICOS (CD278) (clone C398.4A)	BD Biosciences	Cat# 566991; RRID: AB_2869993
BUV563 Mouse anti-human CD25 (clone 2A3)	BD Biosciences	Cat# 612918; RRID: AB_2870203)
Mouse anti-human HLA-DR, PE-Cyanine5.5 (clone TU36)	Thermo Fisher Scientific	Cat# MHLDR18; RRID: AB_10372966
Brilliant Violet 785 anti-human CD14 (clone M5E2)	BioLegend	Cat# 301840; RRID: AB_2563425
BV650 Mouse anti-human CD16 (clone 3G8)	BD Biosciences	Cat# 563692; RRID: AB_2869511
PE/Cyanine7 anti-human CD11c A (clone 3.9)	BioLegend	Cat# 301608; RRID: AB_389351
PE/Cyanine5 anti-human CD123 (clone 6H6)	BioLegend	Cat# 306008; RRID: AB_493574
Brilliant Violet 605 anti-human CD183 (CXCR3) (clone G025H7)	BioLegend	Cat# 353728; RRID: AB_2563157
Brilliant Violet 510 anti-human CD194 (CCR4) (clone L291H4)	BioLegend	Cat# 359416; RRID: AB_2562437
Brilliant Violet 711 anti-human CD279 (PD-1) (clone EH12.2H7)	BioLegend	Cat# 329928; RRID: AB_2562911
BUV395 Mouse anti-human CD107a (clone H4A3)	BD Biosciences	Cat# 565113; RRID: AB_2739073
Anti-human Granzyme B, PE-Cyanine5.5 (clone GB11)	Thermo Fisher Scientific	Cat# GRB18; RRID: AB_2536541
Anti-human CD30 Ligand/TNFSF8 PE (clone 116614)	R and D Systems	Cat# FAB1028P; RRID: AB_2207494
BV421 Mouse anti-human CD154 (clone TRAP1)	BD Biosciences	Cat# 563886; RRID: AB_2738466
Brilliant Violet 510 anti-human CD127 (IL-7R) (clone A019D5)	BioLegend	Cat# 351332; RRID: AB_2562304
PE-Cy7 Mouse anti-human CD45RA (clone L48)	BD Biosciences	Cat# 337167; RRID: AB_647424
PE-Cy7 Mouse anti-human CD45RA (clone 5H9)	BD Biosciences	Cat# 561216; RRID: AB_10611721
BUV395 Mouse anti-human CD45RA (clone 5H9)	BD Biosciences	Cat# N/; RRID: AB_2740052
BV421 Mouse anti-human IL-21 (clone 3A3-N2.1)	BD Biosciences	Cat# 564755; RRID: AB_2738933)
Anti-CD4 monoclonal antibody, PE-Cyanine5.5 (clone S3.5)	Thermo Fisher Scientific	Cat# MHCD0418; RRID: AB_10376013
BUV737 Mouse anti-human CD4 (clone SK3)	BD Biosciences	Cat# 564305; RRID: AB_2713927)
BV711 Mouse anti-human Invariant NK T Cell (clone 6B11)	BD Biosciences	Cat# 747720; RRID: AB_2872199
Brilliant Violet 785 anti-human CD279 (PD-1) (clone EH12.1)	BioLegend	Cat# 329930; RRID: AB_2563443
FcR Blocking Reagent, human	Miltenyi Biotec	Cat# 130-059-901; RRID: AB_2892112
Rhesus macaque MR1 (5-OP-RU), biotinylated monomer	NIH Tetramer Core Facility	N/A
Brilliant Violet 421 Streptavidin	Biolegend	Cat# 405225
Brilliant Stain Buffer Plus	BD Biosciences	Cat# 566385
LIVE/DEAD Fixable Blue Dead Cell Stain Kit, for UV excitation	Thermo Fisher Scientific	Cat# L23105

(Continued on next page)

Continued

REAGENT or RESOURCE	SOURCE	IDENTIFIER
Cytofix/Cytoperm Plus Fixation/Permeabilization Solution Kit with BC GolgiPlug	BD Biosciences	Cat# 555028
eBioscience Protein Transport Inhibitor Coctail	Thermo Fisher Scientific	Cat# 00-4980-03
Anti-human/monkey IFNg mAb (clone MT126L)	MABTECH	Cat# 3421M-3-250
Anti-human IFNg mAb (clone 7-B6-1)	MABTECH	Cat# 3420-6-250
Streptavidin-HRP	MABTECH	Cat# 3310-1000
AEC Substrate kit, HRP	Vector Laboratories	SK-4200
Bacterial and virus strains		
BCG SSI (Danish strain 1331)	Aeras (IAVI)	Lot# 050613MF
Mtb Erdman barcode library	BEI Resources	Cat# NR-50781
Biological samples		
Rhesus macaque blood, BAL, and tissues	This study	N/A
Chemicals, peptides, and recombinant proteins		
Mtb H37Rv whole cell lysate	BEI Resources	Cat# NR-14822
Tuberculin PPD	(Statens Serum Institut)	Batch RT50
Peptide array, Mtb ESAT-6 protein	BEI Resources	Cat# NR-50711
Peptide array, Mtb CFP-10 protein	BEI Resources	Cat# NR-50712
Mtb H37Rv Culture Filtrate Protein (CFP)	BEI Resources	Cat# NR-14825
Mtb300 Megapool	Aeras/JPT	Batch 040917Sass-01
Critical commercial assays		
Milliplex Map Non-human primate cytokine magnetic bead panel -Immunology multiplex assay	Millipore Sigma	Cat# PRCYTOMAG-40K
Deposited data		
Custom code used for analysis	This paper	Zenodo.org; record number 7855102
Software and algorithms		
OsiriX MD v12.0.3	Pixmeo SARL	RRID:SCR_013618
GraphPad Prism v9.3.1	GraphPad	RRID:SCR_002798
Flowjo v.9.9.8 and 10.8.1	BD Biosciences	RRID:SCR_008520
FACS Diva	BD Biosciences	RRID:SCR_001456
SPICE v6.1	https://niaid.github.io/spice/	RRID:SCR_016603
JMPPro v14.3.0	SAS Institute Inc.	RRID:SCR_014242
R project for Statistical Computing v4.0.2	R Core Team	RRID:SCR_001905
R package – dplyr v 1.0.5	CRAN	https://cran.r-project.org/web/packages/dplyr/
R package – ggplot2 v3.3.5	CRAN	https://cran.r-project.org/web/packages/ggplot2/index.html
R package glmnet v4.1.4	CRAN	https://cran.r-project.org/web/packages/glmnet/index.html
R package systemsseRology	GitHub	https://github.com/LoosC/systemsseRology
R package – Hmisc v4.4.2	CRAN	https://cran.r-project.org/web/packages/Hmisc/index.html

(Continued on next page)

Continued

REAGENT or RESOURCE	SOURCE	IDENTIFIER
R package – Stats v4.0.3	CRAN	https://rdrr.io/r/stats/stats-package.html
R package- ggraph v2.0.4	CRAN	https://cran.r-project.org/web/packages/ggraph/index.html
R package igraph v 1.2.6	CRAN	https://cran.r-project.org/web/packages/igraph/index.html
R package lme4 v 1.1.29	CRAN	https://cran.r-project.org/web/packages/lme4/index.html
R package ggpubr v0.4.0	CRAN	https://cran.r-project.org/web/packages/ggpubr/index.html
R package rstatix v07.0	CRAN	https://cran.r-project.org/web/packages/rstatix/index.html
R package caret v6.0.92	CRAN	https://cran.r-project.org/web/packages/caret/vignettes/caret.html
Other		
LSR Fortessa X-50 Cell Analyzer	BD Biosciences	RRID:SCR_019602
LSR II Flow Cytometer	BD Biosciences	RRID:SCR_002159
Immunospot Plate Reader	Cellular Technology International, Inc.	Cat#S6MACRO
Bio-Plex MAGPIX Multiplex Reader	Bio-Rad	N/A
Luminex FLEXMAP 3D Instrument System	Thermo Fisher Scientific	Cat# APX1342
MultiScan LFER150 PET/CT	Mediso	N/A
MicroPET Focus 220 preclinical PET scanner	Siemens	N/A
Cremltom CT scanner (clinical 8-slice)	NeuroLogica	N/A
GentleMACS Tissue Dissociator	Miltenyi	RRID:SCR_020267

RESOURCE AVAILABILITY

Lead contact

Further information and requests for resources and reagent should be directed to and will be fulfilled by the lead contact, Mario Roederer (mario@mail.nih.gov).

Materials availability

This study did not generate new unique reagents.

Data code and availability

- The dataset generated during and/or analyzed during the current study have been made available in the [supplemental information](#).
- Custom code was used in this manuscript and has been made available at [Zenodo.org](#) under the record number 7855102. The R packages used for data analysis are described in more detail in the [STAR Methods](#) section and the [key resources table](#).
- Any additional information required to reanalyze the data reported in this paper is available from the lead contact upon request.

EXPERIMENTAL MODEL AND SUBJECT DETAILS

Animals

Animal work was approved by the Institutional Care & Use Committees of AAALAC (American Association for Accreditation of Laboratory Animal Care)-accredited institutions (NIH Vaccine Research Center, Bioqual, Inc., and the University of Pittsburgh) and determined to be in accordance with the guidelines outlined by the Animal Welfare Act and Regulation (USDA) and the Guide for the Care & Use of Laboratory Animals, 8th Edition (NIH).

35 adult Indian-origin rhesus macaques (*Macaca mulatta*; median age 4.7 years; 17 males and 18 females) were housed throughout the vaccination phase at Bioqual, Inc. and transferred to the University of Pittsburgh (ABSL-3) for the challenge phase. Animals were monitored for physical health, food consumption, body weight, temperature (rectal probe), complete blood counts, and serum chemistries. MHC alleles were determined by sequencing (available upon request).

METHOD DETAILS

Study design

The study design (Figure S1) included 6 vaccine groups receiving half-log increments of i.v. BCG over a 3-log dose range ($4.5 \log_{10}$ - $7.5 \log_{10}$ CFU) and one unvaccinated control. The sample size of each dose group was assigned with a goal of achieving 50% protection overall. We predicted that protection would begin to diminish within $1 - 1.5 \log_{10}$ CFU below our published protective i.v. BCG dose ($7.64 \log_{10}$ mean CFU) and therefore assigned most of the animals in cohort (a) to dose groups of $6 - 7 \log_{10}$ CFU. After analyzing the protective outcome of cohort (a), we elected to add a second cohort of animals (b) that would receive lower doses ($5 - 6 \log_{10}$ CFU) of i.v. BCG. Animals were randomized into vaccine groups based on birth colony, gender, and pre-vaccination CD4 T cell responses to PPD in the BAL. Post-hoc analysis of MHC alleles revealed no association with protection.

BCG vaccination

Animals were vaccinated at Bioqual, Inc. under sedation. BCG Danish Strain 1331 (Statens Serum Institute) that had been expanded and cryopreserved by Aeras (now IAVI) was serially diluted in cold PBS containing 0.05% tyloxapol (Sigma-Aldrich) and delivered intravenously into the saphenous vein in a volume of 2ml. Actual BCG doses were quantified by dilution-plating and are reported in Figure S1A.

Mtb challenge

Macaques were challenged 5 - 6 months after i.v. BCG vaccination by delivering a 2ml volume of PBS containing an average of 12 CFU (range 4 - 17 CFU) of barcoded Mtb Erdman as described.³⁰ Actual Mtb doses were quantified by plating and reported in Table S1. Infectious doses across this range result in similar levels of TB disease in unvaccinated rhesus macaques in this and previous studies. Clinical monitoring of appetite, behavior, body weight, and cough and serial erythrocyte sedimentation rate and Mtb growth from gastric aspirate assessments were performed. These signs and PET CT characteristics were used to determine whether a macaque met humane endpoint criteria prior to the study endpoint.

Sample processing

Blood and BAL were collected according to the schedule in Figure S1B. Blood PBMC were separated using Ficoll-Paque PLUS and cryopreserved in FBS containing 10% DMSO; plasma was collected after ficoll separation. BAL wash fluid (3 x 20 ml washes with PBS) was centrifuged and the supernatant was collected and frozen. BAL cells were resuspended in warm R10 (RPMI 1640 with 2 mM L-glutamine, 100 U ml⁻¹ penicillin, 100 µg ml⁻¹ streptomycin, and 10% heat-inactivated FBS) containing 50U/ml benzonase and passed through a 70 µM cell strainer before counting.

Multiparameter flow cytometry

BAL cells were analyzed fresh on the day of collection while PBMCs were cryopreserved and batch-analyzed at the end of the study. For BAL, $1-5 \times 10^6$ cells per sample were either stained immediately (unstimulated) or stimulated with R10 alone or 20 µg ml⁻¹ Tuberulin PPD (Statens Serum Institut) for 2 h before adding 10 µg ml⁻¹ BD GolgiPlug and incubating for an additional 12 h at 37°C before staining. For PBMC, cryopreserved cells were thawed, washed in R10 and either stained immediately (unstimulated) or rested in R10 for 7 h prior to stimulation. $1-3 \times 10^6$ PBMCs were incubated for 14 h at 37°C (12 h with eBioscience Protein Transport Inhibitor Cocktail) with R10 alone, 20 µg ml⁻¹ Mtb H37Rv whole cell lysate (WCL, BEI Resources), 2 µg ml Mtb300 peptides,³¹ or 1 µg ml⁻¹ each of ESAT-6 and CFP-10 peptide pools (BEI Resources). Antibody and tetramer information and gating strategies for BAL and PBMC flow cytometry panels are shown in Figures S3, S5, S6, and S8. Generally, PBMC and BAL were stained as follows (all steps are at RT; not all steps refer to all panels): Wash twice with PBS/BSA (0.1% BSA); 20 min incubation with tetramer diluted in PBS/BSA (rhesus MR1 tetramer³² was provided by the NIH Tetramer Facility); wash twice with PBS; viability stain in PBS for 20 min; wash twice with flow buffer (PBS containing 0.1% BSA and 0.05% sodium azide); 10 min incubation with human FcR blocking reagent (Miltenyi Biotec); incubation with surface marker antibody cocktail in flow buffer containing 1x BD Brilliant Stain Buffer Plus for 20 min; wash thrice with flow buffer; 20 min incubation BD Cytofix/Cytoperm solution; wash twice with 1x BD Perm/Wash buffer; 30 min incubation with intracellular antibody cocktail in Perm/Wash Buffer containing 1x BD Brilliant Stain Buffer Plus; wash thrice with Perm/Wash buffer. Samples were acquired on either a BD LSR II cytometer or a BD LSRFortessa X-50 and analyzed with FlowJo Software (v.9.9.8 or 10.8.1 BD Biosciences) as previously described.⁷

ELISpot and milliplex assays

For ELISpot, hydrophobic high protein binding membrane plates were hydrated with 40% ethanol, washed with sterile water, and coated with anti-human/monkey IFNγ antibody (15 µg mL⁻¹, MT126L, MabTech) overnight at 4°C. Plates were washed with PBS and blocked with RPMI plus 10% human AB serum for 2 h at 37°C with 5% CO₂. 2×10^5 PBMCs per well were incubated in

RPMI supplemented L-glutamate, HEPES and 10% human AB serum alone (negative control) or containing 1 μ g mL $^{-1}$ each of ESAT-6 or CFP-10 peptide pools (BEI Resources) or 2 μ g mL $^{-1}$ Mtb culture filtrate protein (CFP) for 40–48 h. To develop, plates were washed with PBS and biotinylated anti-human IFN γ antibody (2.5 μ g mL $^{-1}$, 7-B6-1, MabTech) was added for 2 h at 37°C. After washing, streptavidin-HRP (1:100, MabTech) was added for 45 min at 37°C. Spots were stained using AEC peroxidase (Vector Laboratories, Inc.) and counted manually on an ELISpot plate reader. Data are reported as average spots from duplicate background subtracted wells. Wells with confluent staining were described as too numerous to count (TNTC). The cutoff for a positive ELISpot response was 10 SFU/200,000 PBMC, determined by assessing results prior to infection in this and previous studies. For plasma cytokine measurement: cryopreserved plasma samples were batch-analyzed using a MILLIPLEX NHP cytokine multiplex kit per instructions (Millipore Sigma) and analyzed on a Bio-Plex Magpix Multiplex Reader (Bio-Rad).

Antibody levels

LAM- and PPD-specific antibody levels were measured as described previously.¹¹ In brief, LAM and PPD were coupled to magnetic Luminex beads by DMTMM modification,³³ and carbodiimide-NHS ester coupling,²¹ respectively. Coupled beads were incubated with plasma and BAL overnight at 4°C in 384-well plates (Greiner Bio-One) using the following dilutions: plasma IgG1 (1:30 for PPD, 1:150 for LAM), plasma IgA (1:30), and plasma IgM (1:750). Following overnight incubation, the plates were washed and unconjugated mouse anti-rhesus IgG1 (clone 7H11), IgA (clone 9B9), or IgM (Life Diagnostics, clone 2C11-1-5) antibody was added and incubated shaking at RT for 1 h. Anti-rhesus IgG1 and IgA were obtained from the National Institutes of Health Nonhuman Primate Reagent Resource. After the secondary incubation, plates were washed and phycoerythrin (PE)-conjugated goat anti-mouse IgG was added (ThermoFisher, 31861) and incubated shaking at RT for 1 h. Plates were washed and relative antibody levels (PE MFI values) were measured using a FlexMap 3D (Luminex). Data are represented as the log₂ fold change in MFI over the pre-vaccination level for each animal. Samples were measured in duplicate.

PET CT scans and analysis

PET CT scans were performed using a microPET Focus 220 preclinical PET scanner (Siemens Molecular Solutions) and a clinical eight-slice helical CT scanner (NeuroLogica Corporation), or a preclinical integrated PET CT MultiScan LFER 150 (Mediso Medical Imaging Systems). 2-deoxy-2-(¹⁸F)Fluorodeoxyglucose (FDG) was used as the PET probe. PET CT scans prior to Mtb challenge (23 of 34 vaccinated macaques; 1 unvaccinated) revealed no lung FDG activity (inflammation) although 8 of the 23 vaccinated animals had 1–4 thoracic lymph nodes with “warm” FDG activity (Standard Uptake Value; SUV >2.3 but <5) and 1 vaccinated animal had a single “hot” LN (SUV >5). However, there was no association between FDG activity and IV BCG dose. PET CT scans were performed on all animals 4, 8, and ~12 weeks (necropsy) after Mtb challenge. OsiriX MD (v.12.0.3) was used for scan analyses, as described.³⁴ Lung inflammation was measured as total FDG activity in lungs. A region of interest (ROI) was segmented which encompassed all lung tissue on CT and was then transferred to the co-registered PET scan. On the PET scan, all image voxels of FDG-avid pathology (SUV > 2.3) were isolated and summated resulting in a cumulative standardized uptake value. To account for basal metabolic FDG uptake, total FDG activity was normalized to resting muscle resulting in a total lung inflammation value. Individual granulomas were counted on each CT scan. If granulomas were too small and numerous within a specific area to count individually or if they consolidated, quantification was designated too numerous to count (TNTC).

Necropsy, pathology scoring, and Mtb burden

10–12 weeks after Mtb infection or at humane endpoint, macaques were euthanized by sodium pentobarbital injection, followed by gross examination for pathology. A published scoring system was used to determine total pathology from each lung lobe (number and size of lesions), lymph nodes (LN; size and extent of necrosis), and extrapulmonary compartments (number and size of lesions and whether the sample was CFU+).²³ Granulomas and other lung pathologies, all thoracic LNs, and peripheral LNs were matched to the final PET-CT scan and collected for quantification of Mtb. Each lesion in the lung (including granulomas, consolidations, and granuloma clusters), all thoracic LNs, random sampling (50%) of each of the seven lung lobes, spleen, and liver (3–5 granulomas if present or random samples (30%)), and any additional pathologies were processed to comprehensively quantify bacterial burdens. Sample processing was as follows: lung and spleen samples were processed using gentleMACS C tubes in RPMI 1640 followed by passing through a 70 μ M cell strainer; LNs and granulomas and other lung lesions were mechanically disrupted and filtered through a cell strainer. Individual samples were plated on 7H11 agar and incubated at 37°C with 5% CO₂ for 3 weeks for CFU enumeration or formalin-fixed and paraffin-embedded for histological examination. CFUs were counted and summed to calculate the total thoracic bacterial burden for the animal. Three Mtb-infected animals with extensive PET CT readings were not necropsied and instead, total thoracic CFU was estimated based off PET CT activity, using a linear regression model equation developed previously.²³ Values were only estimated and included for total CFU and thus these animals were excluded from lung, LN and extrapulmonary CFU analysis, but these animals were considered unprotected. Bacterial burden data for each macaque are listed in Table S1.

QUANTIFICATION AND STATISTICAL ANALYSIS

Data preprocessing

Immune measurements comprising values not above the noise level (e.g., Boolean subsets of antigen-specific CD4 T cells in PBMC that did not express CD154), the values for those measurements and their dependent features (e.g., the phenotype of such antigen-specific CD154⁻CD4 T cells) were excluded. This eliminated 650 of 2,673 measured values. Then, for all immune measurements collected longitudinally, the normalized area under the curve (nAUC) was computed as a time-weighted average value. This further reduced the number of features to 376, including PBMC, BAL, and complete blood counts (CBC). The nAUC method was chosen to reduce the total number of features as well as reducing noise by virtue of time-averaging.

Quantification and statistics

Dot plots were created in Graphpad Prism (v.9.3.1 for macOS) to visualize outcomes by binned BCG dose. Kendall's τ was used to test if there was a correlation between dose (\log_{10} -transformed) and each of the continuous outcomes. Fisher's exact test was used to test the difference of proportions for two categorical variables (proportion of sterile animals). Nominal logistic regression models were used to test whether T cells in the airways predict protection (with \log_{10} -transformed dose added as a fixed effect). Nominal regression models were also used to test whether T cells in uninvolvled lung lobes predict protection. Kendall's τ and logistic regression models were calculated in JMP®Pro (v.14.3.0). Fisher's exact test was calculated in Graphpad Prism.

Polar plot

Polar plots show the mean percentile of each measurement across the protected and non-protected groups in different compartments. First, percentile rank scores were calculated for each measurement in all samples using the 'percent rank' function of the R package dplyr v1.0.5. Then, the mean percentiles were determined using the samples corresponding to protected and non-protected groups, respectively. The plots are visualized by the 'ggplot' function in R package ggplot2 v.3.3.5).

Multivariate modeling

Models were built with an approach using a combination of the LASSO (Least Absolute Shrinkage and Selection Operator) for feature selection and then classification using PLSDA (Partial Least Square Discriminant Analysis) with the LASSO-selected features.²⁴ For the input of the combined approach, the nAUC dataset was z-scored. LASSO-based feature selection was performed on logistic regression using the 5-fold cross-validation and was repeated 10 times, and features, which are selected 5 times out of 10, were identified as selected features. Using the selected features, PLSDA was performed to discriminate protected animals from non-protected ones using the selected features with the corresponding groups. The first 2 latent variables (LVs) from a PLSDA model trained on the LASSO-selected features were visualized. LVs are compound variables composed of the LASSO-selected features. For visualization, 95% of data ellipses were calculated. Features were ordered according to their variable importance in projection (VIP) score, a score that is higher for features that contribute more to the model. Model robustness was assessed using 8-fold cross-validation. For each cross-validation run, the animals were randomly stratified into 8 subsets, ensuring that both groups were represented in each subject, with 7 subsets serving as the training set and the left one as the test set. Each subset served as the test set once. Then the average cross-validation accuracy was reported for 10 repetitions. In each cross-validation repetition, the significance of model performance was evaluated using "negative control" models of permuted testing by randomly shuffling the group labels. This process was repeated 100 times to generate a distribution of model accuracies. Then, the P values were obtained as the tail probability of the true classification accuracy from the cross-validation model in the distribution of the classification accuracies from permutation testing experiments. Finally, the median P value across 10 repetitions was reported with a resolution of 0.01. It was worth mentioning that "P < 0.01" means that the true classification accuracy is higher than all the accuracies across 100 times. In addition, the average confusion matrix was generated by five-fold cross-validation strategies 100 times to evaluate the robustness of the PLSDA model based on the selected representative features. The average confusion matrix across 100 simulations was visualized. LASSO was performed using R package glmnet v.4.1.4 and PLS-DA models were generated with the R package rpls interfaced by R package systemsRology. The analyses were performed with R version 4.0.2.

Correlation networks

Correlation networks were constructed to visualize the additional measured features that were significantly linked to the selected minimal features by LASSO. In brief, measured features that were significantly correlated with a Holms-Bonferroni correction to the final selected PLS model selected features were defined as co-correlates. Significant Spearman correlations above a threshold of $|r| > 0.7$ were visualized within the networks. Spearman correlation coefficients were calculated using the rcorr function in R package Hmisc v.4.4.2 and the p values were corrected by "Benjamini-Hochberg" correction in R package stats v.4.0.3. For visualization, the correlation networks were displayed using R package ggraph v.2.0.4 and igraph v.1.2.6.

Linear mixed modeling

We used two nested mixed linear models (null and full model) without/with protection information to assess the significance of the association between measurements and protection group while controlling for potential confounding characteristics including the BCG dose and the vaccination cohort. We fit two mixed linear models and estimated the improvement in model fit by likelihood ratio testing to identify the associated measurements.

Null Model: measurement $\sim 1 + \log_{10}(\text{IV.BCG.Dose}) + (1 | \text{Cohort})$

Full Model: measurement $\sim 1 + \log_{10}(\text{IV.BCG.Dose}) + \text{Protection?} + (1 | \text{Cohort})$

Likelihood ratio test: $\text{LRT} = -2 * \ln (\text{MLE in Full model} / \text{MLE in Null model}) \sim \chi^2$

The R package lme4 was used to fit the mixed linear model to each measurement and test for differences in measurements depending on whether the NHMs was protected or not based on the total CFU. The *P*-value from the likelihood ratio test and *t* value (normalized coefficients) associated with the variable represented protection/non-protection information, *Protection?* in the full model, were visualized in a volcano plot using the ggplot function in R package 'ggplot2' v. 3.3.5.

Supplemental information

Airway T cells are a correlate of

**i.v. Bacille Calmette-Guerin-mediated protection
against tuberculosis in rhesus macaques**

Patricia A. Darrah, Joseph J. Zeppa, Chuangqi Wang, Edward B. Irvine, Allison N. Bucsan, Mark A. Rodgers, Supriya Pokkali, Joshua A. Hackney, Megha Kamath, Alexander G. White, H. Jacob Borish, L. James Frye, Jaime Tomko, Kara Kracinovsky, Philana Ling Lin, Edwin Klein, Charles A. Scanga, Galit Alter, Sarah M. Fortune, Douglas A. Lauffenburger, JoAnne L. Flynn, Robert A. Seder, Pauline Maiello, and Mario Roederer

Figure S1

A

	Current IV BCG Dose Ranging Study								Historical IV BCG Study	
Binned BCG dose (\log_{10} CFU)	Unvax	4.5 – 5.0	5.0 – 5.5		5.5 – 6.0		6.0 – 6.5	6.5 – 7.0	7.0 – 7.5	> 7.5
N (per binned dose group)	1	3	11		4		6	6	4	10
Actual BCG dose (CFU)	0	3.9×10^4	1.4×10^5	2.0×10^5	3.1×10^5	4.2×10^5	4.6×10^5	2.5×10^6	7.0×10^6	2.5×10^7
N (per actual dose)	1	3	3	5	1	3	6	6	4	5
Vaccination cohort	b	a	b	a	b	b	a	a	a	H

B

Figure S1. Experimental design and timeline, related to all figures.

(A) 34 rhesus macaques across two cohorts (a, b) were vaccinated with IV BCG at half-log increasing doses between 4.5 and 7.5 (\log_{10}) CFU. 1 animal (cohort b) remained unvaccinated and served as an infection control. Actual (plated) doses of BCG administered and number of animals per actual dose and half-log binned dose group are noted. Data from a historical (H) IV BCG study (Darrah et al., 2020) are used in some analyses (**Figure S12**).

(B) PBMC and BAL were collected before (Pre) and at 2, 4, 8, and 12 weeks after BCG vaccination. Additionally, PBMC were collected at the time of Mtb challenge (week 24) as well as at 4-, 8-, and 12-weeks post-challenge. Animals were challenged 24 weeks after IV BCG vaccination with barcoded Mtb Erdman (4 to 17 CFU) via bronchoscope and were monitored for disease using longitudinal PET CT imaging and PBMC ELISpot, as well as pathological assessment and bacterial quantification at necropsy 12 weeks post-challenge (36 weeks after IV BCG).

Figure S2

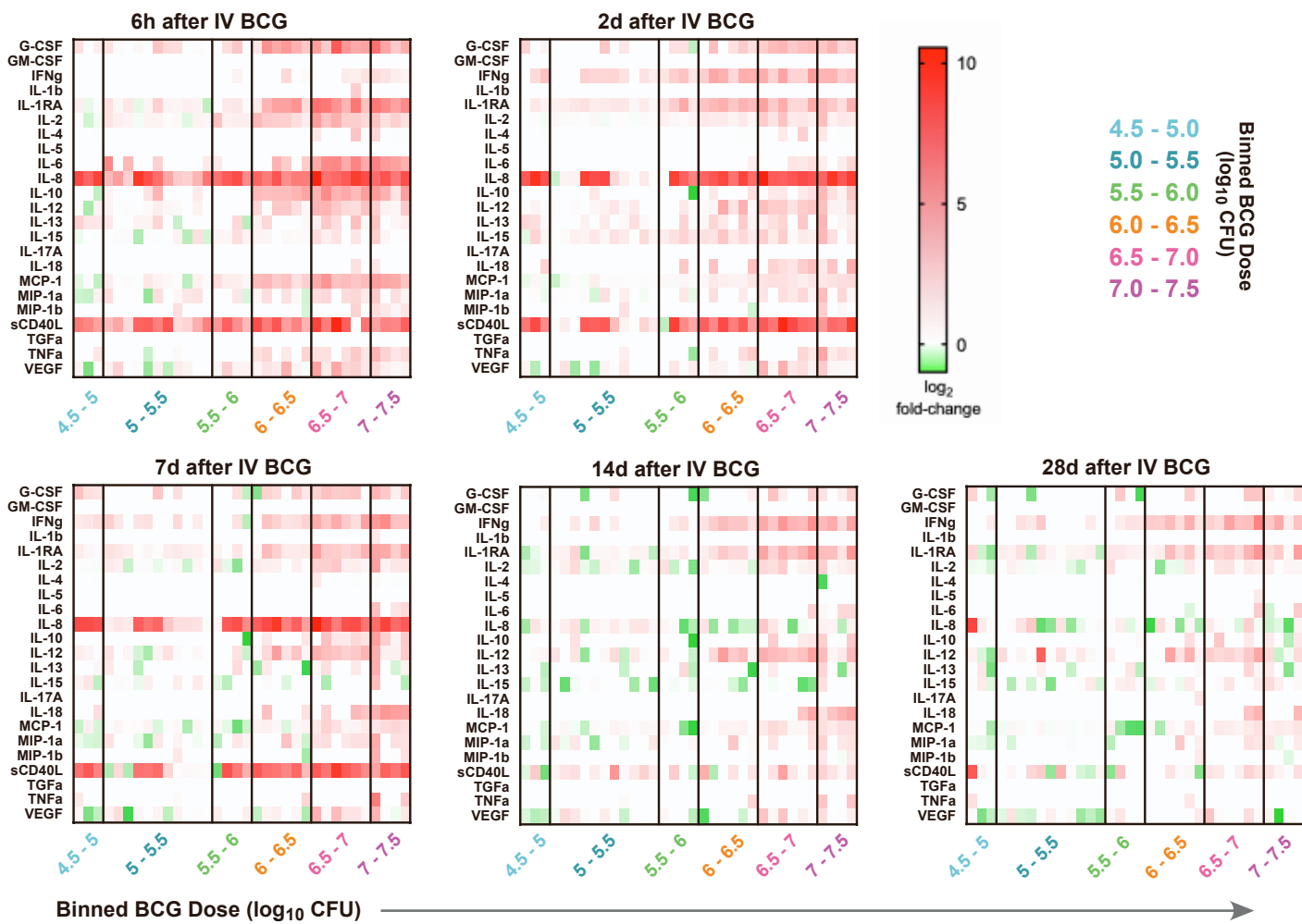
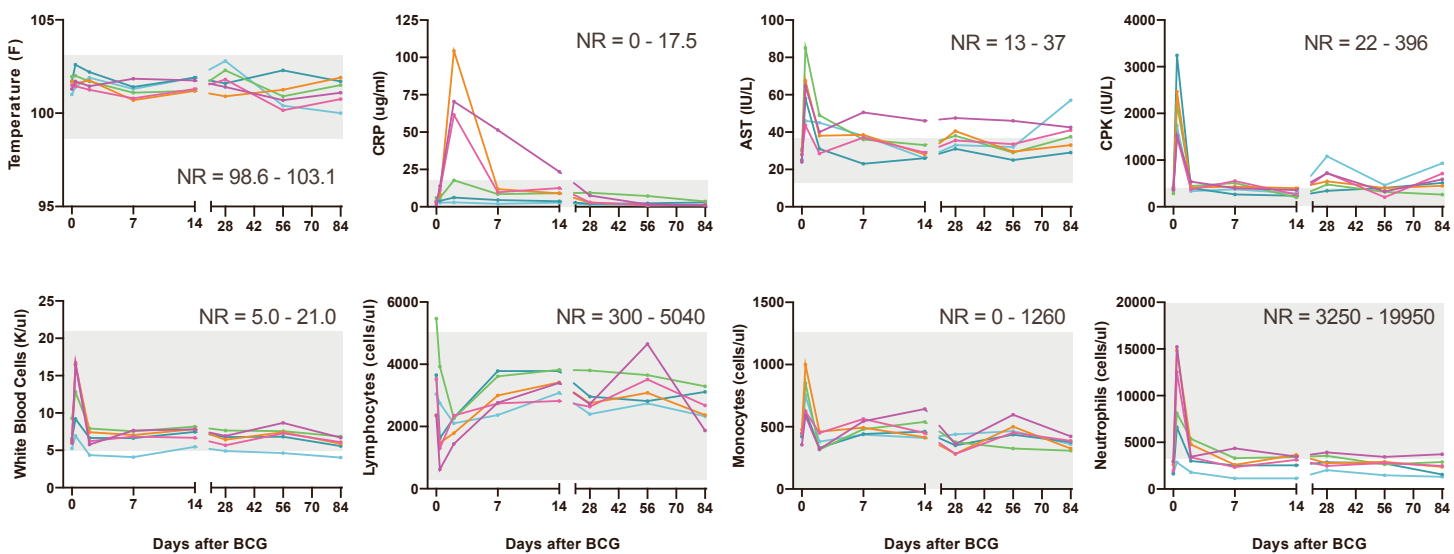
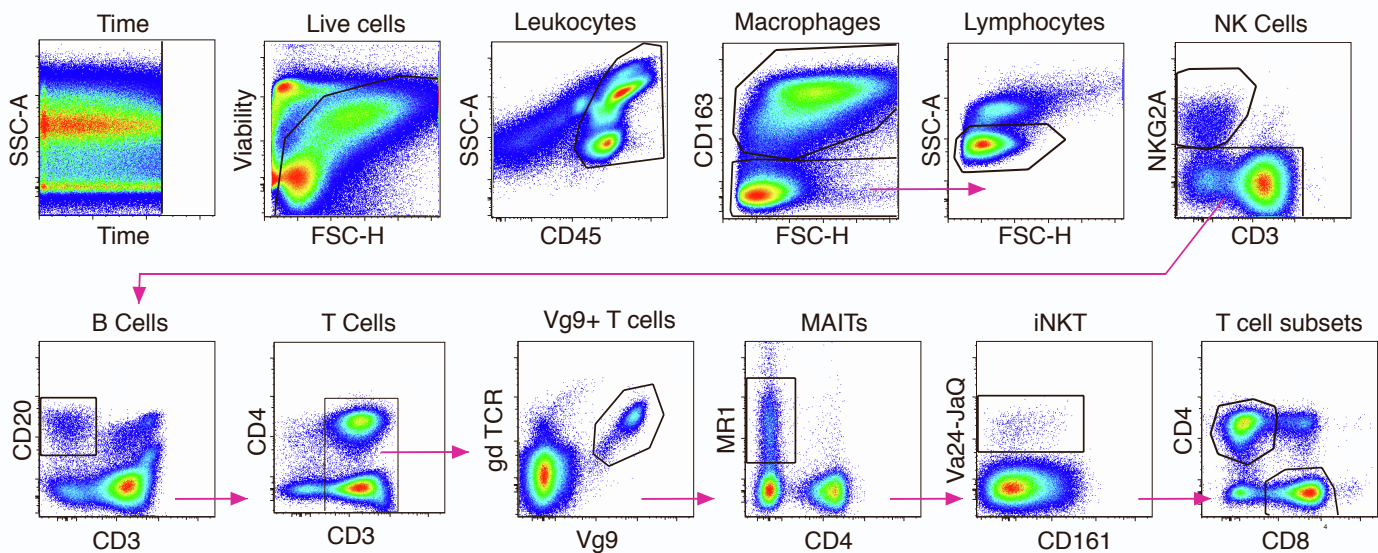
A

B


Figure S2. Systemic cytokine production and clinical parameters after IV BCG vaccination, related to Figure 1.

(A) Cytokines (rows) were measured in the plasma before and after IV BCG vaccination using a 23-plex Luminex assay. Data are shown as \log_2 fold changes over pre-vaccination for each macaque (columns, grouped by binned IV BCG dose) at 6 hours, 2 days, 7 days, 14 days, and 28 days after IV BCG vaccination.

(B) Macaques were monitored for changes in clinical parameters at various time points before and after IV BCG vaccination: temperature; C-reactive protein (CRP) as a marker of inflammation; Liver function (AST); muscle damage (CPK); White blood cells; lymphocytes; monocytes; neutrophils. Data are shown as median values for each dose group. Normal ranges (NR) for rhesus macaques are listed and depicted by shaded area.

Figure S3

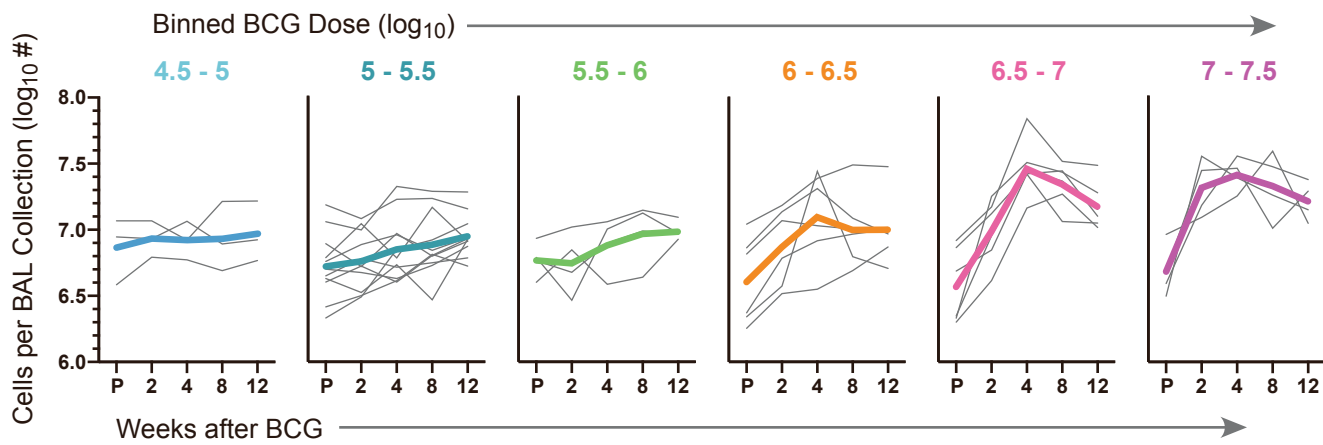
Marker	Clone	Company	Fluorochrome
LIVE/DEAD	Fixable Blue Dead Cell Stain	ThermoFisher Scientific	(U450)
CD45	D058-1283	BD Biosciences	BV510
CD3	SP34-2	BD Biosciences	BV650
CD4	SK3	BD Biosciences	BUV737
CD8	RPA-T8	BD Biosciences	BUV395
TCR $\gamma\delta$	5A6.E9	ThermoFisher Scientific	PE
TCR V γ 9	7A5	ThermoFisher Scientific	Alexa Fluor 680
MR1 tetramer	Rh/5-OP-RU	NIH Tetramer Core	BV421
V α 24-J α Q	6b11	BD Biosciences	BV711
CD69	TP1.55.3	Beckman Coulter	ECD
NKG2A	Z199	Beckman Coulter	APC
HLA-DR	TU36	ThermoFisher Scientific	PE-Cy5.5
CD20	2H7	BioLegend	BV570
CD11b	HP-3G10	BioLegend	BV605
CD163	GHI/61	BioLegend	APC-Cy7
CD14	M5E2	BioLegend	BV785
CD16	3G8	BD Biosciences	BUV496
CD66abce	TET2	Miltenyi Biotec	FITC
CD11c	3.9	BioLegend	PE-Cy7
CD123	6H6	BioLegend	PE-Cy5

Figure S3. Flow cytometry panel for characterization of leukocytes in rhesus BAL, related to Figure 1.

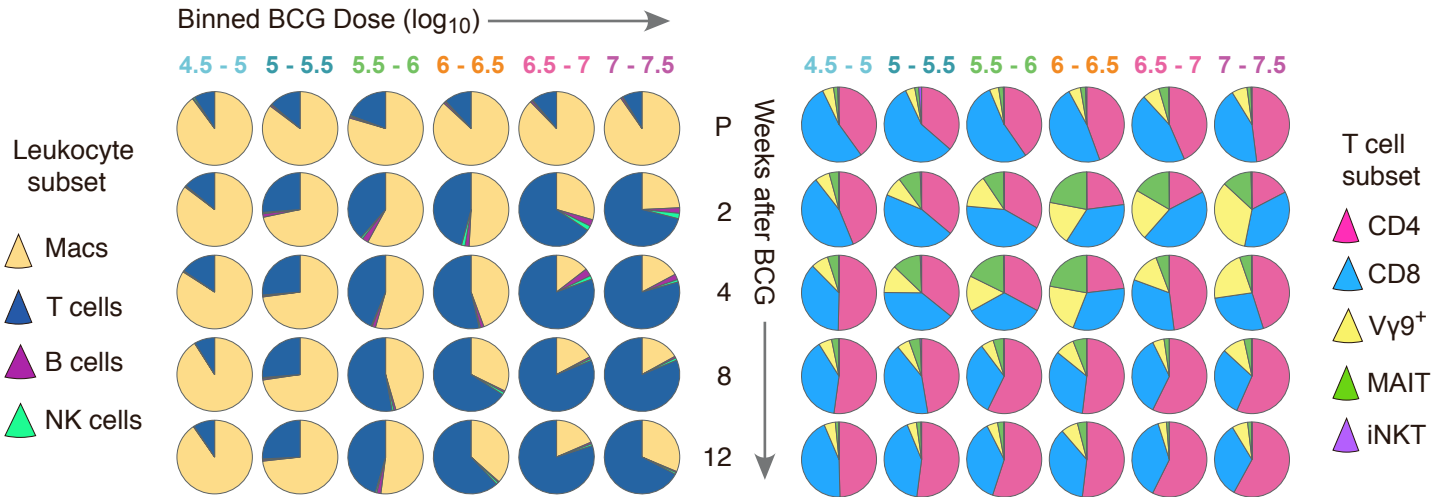
BAL samples were stained for flow cytometry fresh and without stimulation. For each surface marker included in the panel, the antibody clone, source, and fluorochrome are listed. Events were gated by time followed by live leukocyte (CD45+) detection. Macrophages were gated using CD163 and lymphocytes were gated for NK cells (CD3-NKG2A+), B cells (CD3-CD20+) and then total T cells. T cell subsets included V γ 9+ γ δ T cells, MR1-tetramer+ MAIT cells, V α 24-J α Q+ iNKT cells, and conventional CD4 and CD8 T cells.

Figure S4

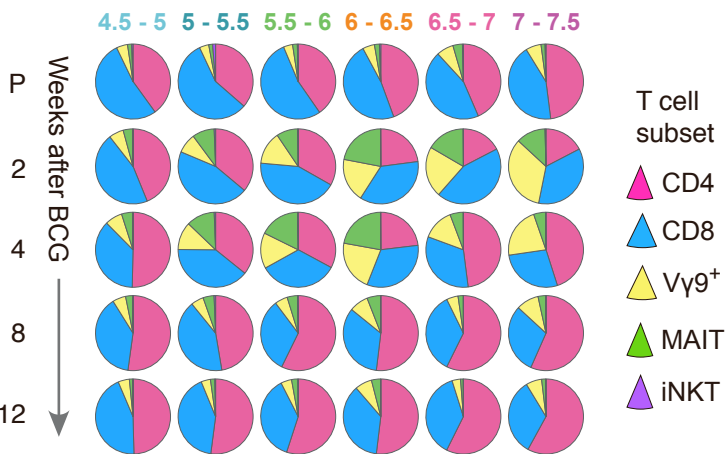
A. BAL



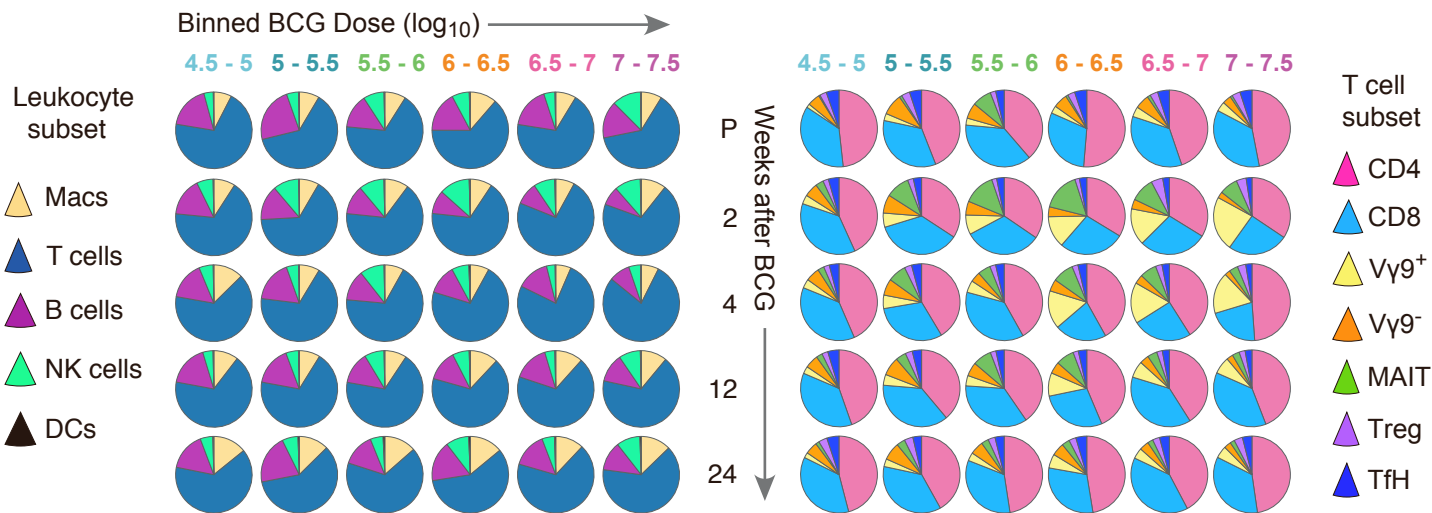
B. BAL



C. BAL



D. PBMC



E. PBMC

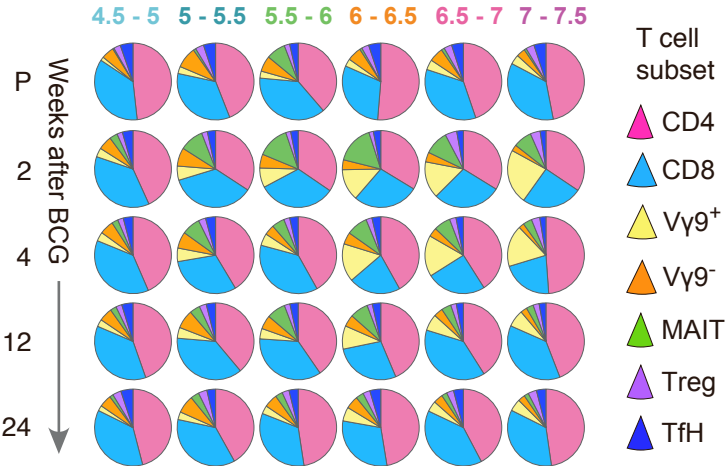


Figure S4. Serial assessment of leukocyte composition in BAL or blood after IV BCG vaccination, related to Figure 1.

(A) Number (\log_{10}) of total live leukocytes per BAL collection before (Pre; P) and at 2, 4, 8, and 12 weeks after IV BCG vaccination as determined by acridine orange/propidium iodide (AO/PI) staining. Shown are data from individual macaques (thin grey lines) and medians (thick colored lines) for each BCG binned dose group.

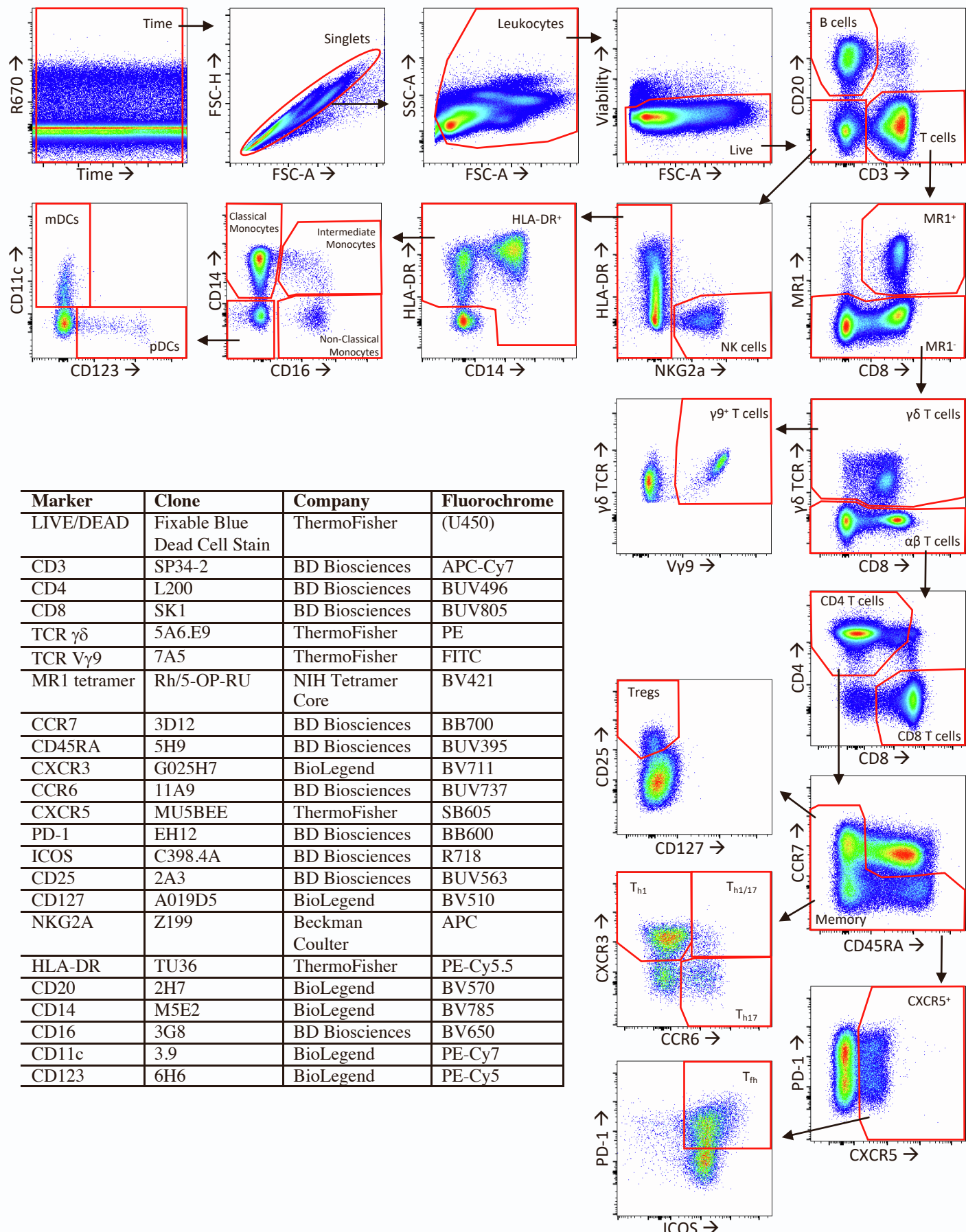
(B) The average proportion of macrophages, T cells, B cells and NK cells within total live leukocytes in BAL as identified by flow cytometry (**Figure S3**) for each dose group (columns) over time (rows).

(C) Proportion of live CD3+ T cells classified as CD4 T cells, CD8 T cells, V γ 9+ γ δ cells, MR1+ MAIT cells, and Vo24+ iNKT cells in BAL as identified by flow cytometry (**Figure S3**).

(D) The average proportion of macrophages, T cells, B cells, NK cells and dendritic cells within total live leukocytes in PBMC as identified by flow cytometry (**Figure S5**) for each dose group (columns) before and up to 24 weeks after BCG (rows).

(E) Proportion of live CD3+ T cells classified as CD4 T cells, CD8 T cells, γ δ T cells (V γ 9+ or V γ 9-), MR1 tetramer+ MAIT cells, CD25+CD127- regulatory T cells (Treg), or CXCR5+ICOS+PD-1+ follicular helper T cells (Tfh) in PBMC as identified by flow cytometry (**Figure S5**).

Figure S5

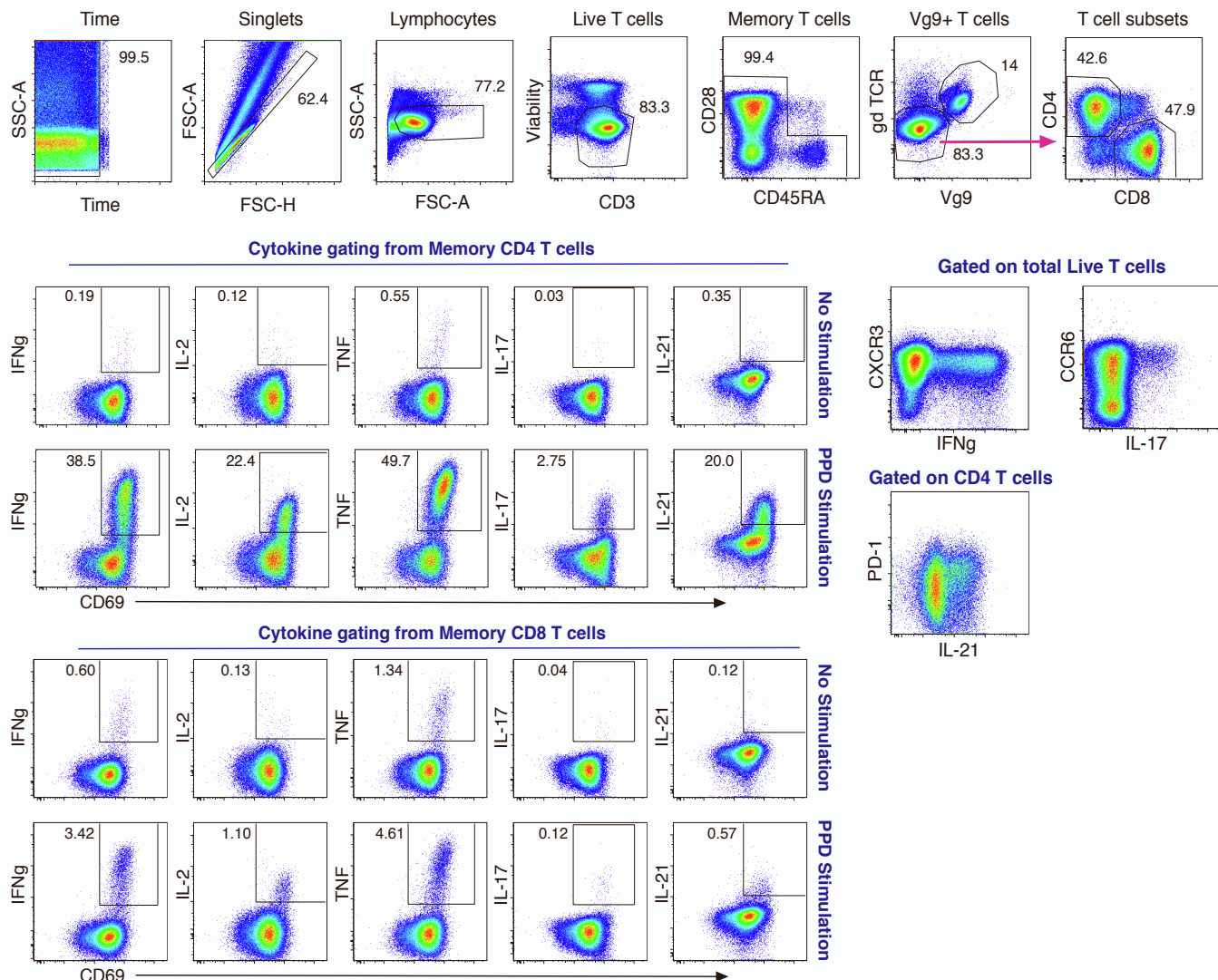


Marker	Clone	Company	Fluorochrome
LIVE/DEAD	Fixable Blue Dead Cell Stain	ThermoFisher	(U450)
CD3	SP34-2	BD Biosciences	APC-Cy7
CD4	L200	BD Biosciences	BUV496
CD8	SK1	BD Biosciences	BUV805
TCR $\gamma\delta$	5A6.E9	ThermoFisher	PE
TCR V γ 9	7A5	ThermoFisher	FITC
MR1 tetramer	Rh/5-OP-RU	NIH Tetramer Core	BV421
CCR7	3D12	BD Biosciences	BB700
CD45RA	5H9	BD Biosciences	BUV395
CXCR3	G025H7	BioLegend	BV711
CCR6	11A9	BD Biosciences	BUV737
CXCR5	MU5BEE	ThermoFisher	SB605
PD-1	EH12	BD Biosciences	BB600
ICOS	C398.4A	BD Biosciences	R718
CD25	2A3	BD Biosciences	BUV563
CD127	A019D5	BioLegend	BV510
NKG2A	Z199	Beckman Coulter	APC
HLA-DR	TU36	ThermoFisher	PE-Cy5.5
CD20	2H7	BioLegend	BV570
CD14	M5E2	BioLegend	BV785
CD16	3G8	BD Biosciences	BV650
CD11c	3.9	BioLegend	PE-Cy7
CD123	6H6	BioLegend	PE-Cy5

Figure S5. Flow cytometry panel for characterization of leukocytes in rhesus PBMC, related to Figure 1.

Cryopreserved PBMC samples were thawed and stained for flow cytometry without stimulation. For each surface marker included in the panel, the antibody clone, source, and fluorochrome are listed. Events were gated by time and then for singlets. Live cells were gated for B cells (CD20+), T cells (CD3+), or non-B/non-T cells. CD20-CD3- cells were gated for NK cells (NKG2A+HLA-DR-); HLA-DR+ cells were divided into monocyte subsets (based on CD14 and CD16) or dendritic cell subsets (based on CD11c or CD123). CD3+ T cells were gated for MR1 tetramer+ CD8+ MAIT cells, V γ 9+ γ δ T cells, or CD4+ and CD8+ T cells. Following total memory selection of CD4 T cells (based on CCR7 and CD45RA), regulatory T cells (T regs) were gated as CD25+CD127 low and T follicular helper cells were gated as CXCR5+PD1+ICOS+. The expression of chemokine receptors associated with Th1 (CXCR3) or Th17 (CCR6) is shown for total memory CD4 T cells.

Figure S6



Marker	Clone	Company	Fluorochrome
Live/Dead	Fixable Blue Dead Cell Stain	ThermoFisher Scientific	(U450)
CD4	S3.5	ThermoFisher Scientific	PE-Cy5.5
CD8	SK1	BD Biosciences	BUV805
Pan $\gamma\delta$ TCR	5A6.E9	ThermoFisher Scientific	PE
TCR V γ 9	7A5	ThermoFisher Scientific	Alexa Fluor 680
CD28	CD28.2	BD Biosciences	PE-Cy5
CD45RA	L48	BD Biosciences	PE-Cy7
CXCR3	G025H7	BioLegend	BV711
CCR6	11A9	BD Biosciences	BUV737
PD-1	EH12	BD Biosciences	BV785
CD3	SP34-2	BD Biosciences	APC-Cy7
CD69	TP1.55.3	Beckman Coulter	ECD
IFN- γ	B27	BD Biosciences	APC
IL-2	MQ1-17H12	BD Biosciences	BV750
TNF	Mab11	BD Biosciences	BV650
IL-17A	BL168	BioLegend	BV570
IL-21	3A3N2.1	BD Biosciences	BV421

Figure S6. Flow cytometry panel to measure antigen-specific T cells in BAL, related to Figure 1.

BAL samples were stained for flow cytometry after *in vitro* stimulation with mycobacterial antigen. For each surface or intracellular (shaded) marker included in the panel, the antibody clone, source, and fluorochrome are listed. Events were gated by time and then for singlets and lymphocytes (based on forward and side scatter). Live CD3+ T cells were gated for total memory T cells using CD28 and CD45RA. After gating V γ 9+ γ δ T cells, CD4 and CD8 T cells were gated. Cytokine staining (IFN γ , IL-2, TNF, IL-17, or IL-21 against CD69) in CD4 and CD8 T cells is shown for a representative unstimulated and PPD stimulated BAL sample. The expression of CXCR3, CCR6, and PD-1 on T cells is also shown for the same stimulated sample.

Figure S7

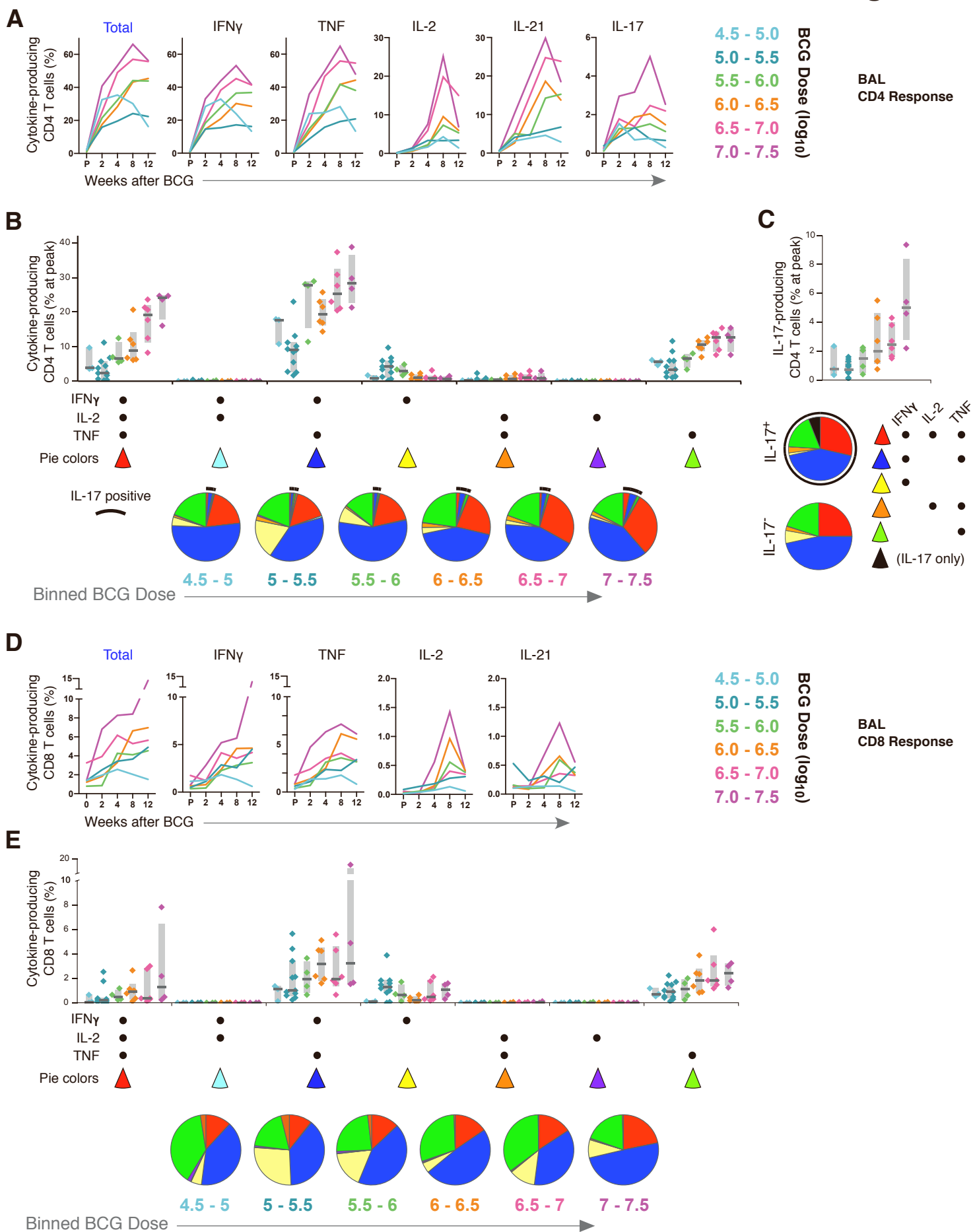


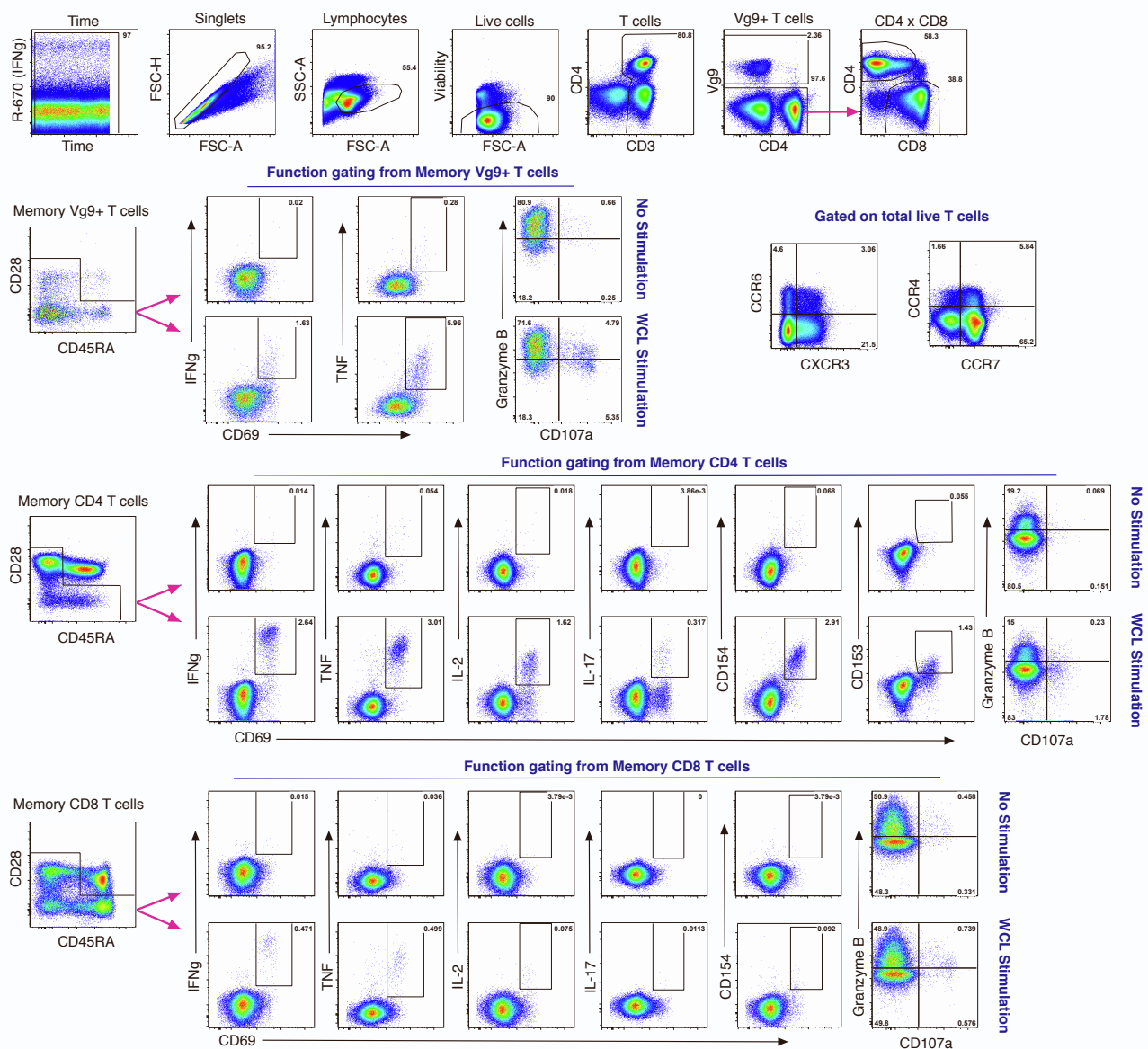
Figure S7. Composition of T cell cytokine responses in BAL after IV BCG immunization, related to Figure 1.

(A, D) Frequencies of memory CD4 **(A)** or CD8 **(D)** T cells in BAL producing IFN γ , TNF, IL-2, IL-21, or IL-17 (any combination (Total), or individual) following *in vitro* stimulation with mycobacterial antigens (WCL) and identified by flow cytometry (**Figure S6**); shown are median responses for each binned dose group before (Pre, P) or 2, 4, 8, and 12 weeks after IV BCG.

(B, E) Peak (8 weeks) antigen-specific CD4 **(B)** and CD8 **(E)** T cell responses were further characterized as the frequency (bar graphs) or proportion (pie graphs) of cells producing every combination of IFN γ , IL-2, or TNF. Frequencies from individual macaques are shown with interquartile range (shaded) and median (horizontal bar). Pie graphs of peak CD4 responses in **(B)** indicate the proportions of IFN γ , IL-2, and TNF production without or with IL-17 production (black pie arcs).

(C) Peak (8 weeks) frequency of IL-17 producing memory CD4 T cells (bar graphs) and the proportions (pie graphs) of IFN γ , IL-2, and TNF production within IL-17-positive (black arc) and IL-17-negative CD4 T cells for all (averaged) dose groups; black pie slice indicates IL-17 single-positive cells.

Figure S8



Marker	Clone	Company	Fluorochrome
LIVE/DEAD	Fixable Blue Dead Cell Stain	ThermoFisher Scientific	(U450)
CD4	L200	BD Biosciences	BUV496
CD8	SK1	BD Biosciences	BUV805
TCR V γ 9	7A5	ThermoFisher Scientific	FITC
CD28	CD28.2	BD Biosciences	PE-Cy5
CCR7	150503	BD Biosciences	Alexa Fluor 700
CD45RA	L48	BD Biosciences	PE-Cy7
CD28	CD28.2	BD Biosciences	PE-Cy5
CXCR3	G025H7	BioLegend	BV605
CCR6	11A9	BD Biosciences	BUV737
CCR4	L291H4	BioLegend	BV510
PD-1	EH12	BD Biosciences	BUV395
CD107a	H4A3	BD Biosciences	APC
CD3	SP34-2	BD Biosciences	APC-Cy7
CD69	TP1.55.3	Beckman Coulter	ECD
IFN- γ	B27	BD Biosciences	APC
IL-2	MQ1-17H12	BD Biosciences	BV750
TNF	Mab11	BD Biosciences	BV650
IL-17A	BL168	BioLegend	BV570
Granzyme B	GRB18	ThermoFisher Scientific	PE-Cy5.5
CD153	116614	R&D Systems	PE
CD154	TRAP1	BD Biosciences	BV421

Figure S8. Flow cytometry panel to measure antigen-specific T cells in PBMC, related to Figure 2.

Cryopreserved PBMC samples were batch-analyzed by flow cytometry after *in vitro* stimulation with mycobacterial antigen. For each surface or intracellular (shaded) marker included in the panel, the antibody clone, source, and fluorochrome are listed. Shown is cytokine production from a representative PBMC sample, with or without WCL stimulation. Events were gated by time and then for singlets and lymphocytes (based on forward and side scatter). Viable lymphocytes were gated for total CD3+ T cells and then gated for V γ 9+ γ δ T cells, CD4 and CD8 T cells. For each T cell subset, memory T cells were selected using CD28 and CD45RA. Depending on production by the individual subset, T cells were gated for production of IFN γ , TNF, IL-2, IL-17, CD154, or CD153 against the activation marker CD69. Granzyme B and CD107 gates were drawn on total T cells but applied only to antigen-specific T cells. Expression of chemokine receptors (CXCR3, CCR6, CCR4, and CCR7) is shown for total T cells.

Figure S9

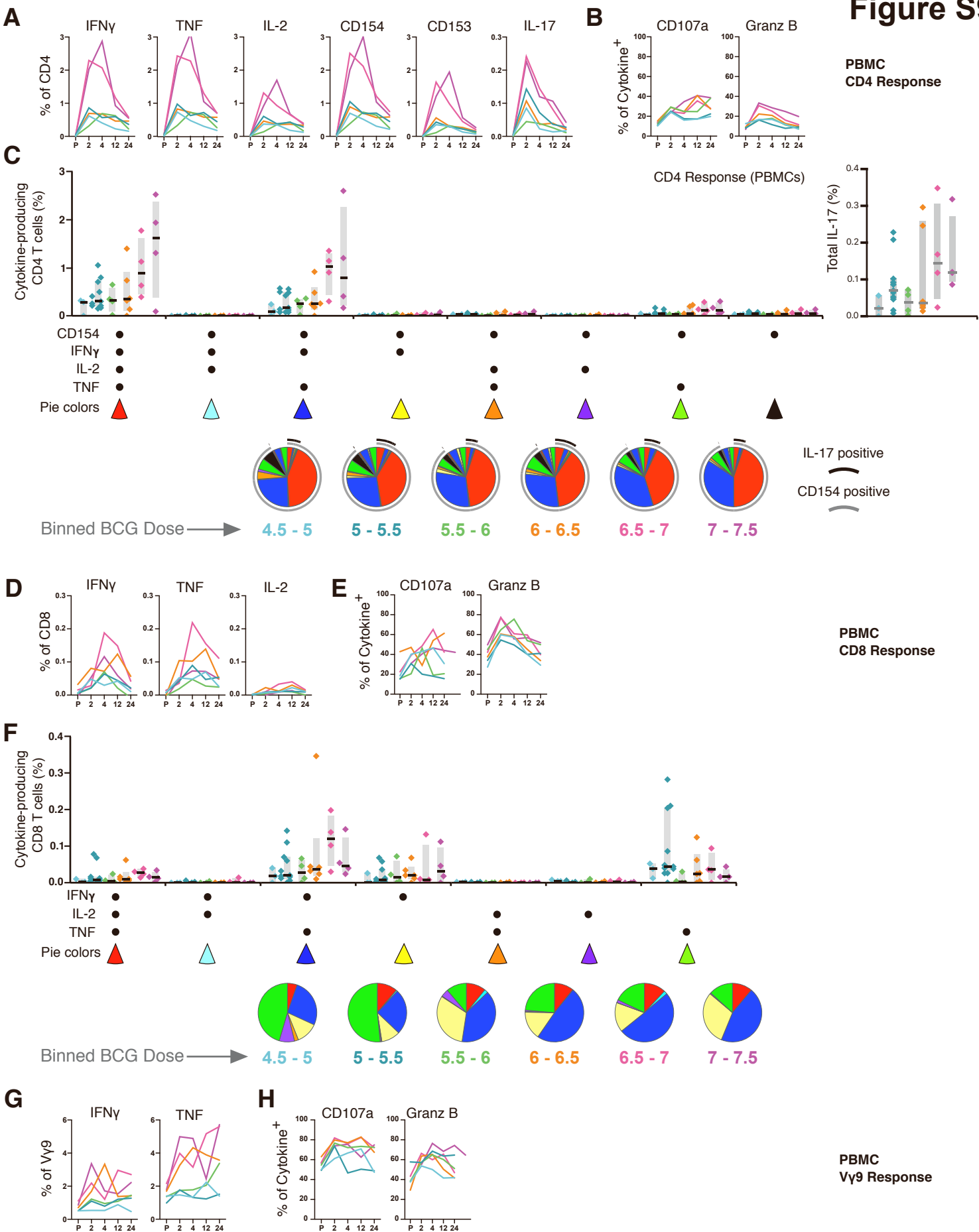


Figure S9. Composition of T cell cytokine response in PBMC after IV BCG immunization, related to Figure 2.

(A, D, G) Frequency of memory CD4 (A), CD8 (D), or V γ 9+ γ δ (G) T cells in PBMC producing IFN γ , TNF, IL-2, CD154, CD153, or IL-17 following *in vitro* stimulation with mycobacterial antigens (WCL) as identified by flow cytometry (Figure S8). Shown are median responses for each IV BCG dose group before (Pre, P) and 2, 4, 12, and 24 weeks after BCG immunization.

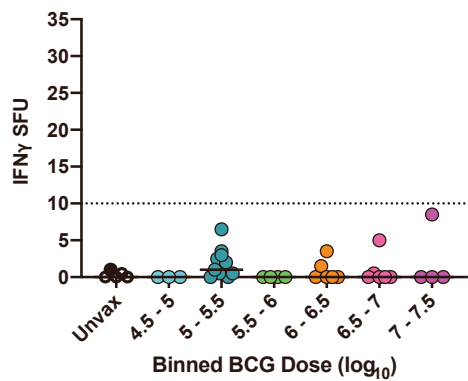
(B, E, H) Percent of mycobacterial-responsive (cytokine-producing) CD4 (B), CD8 (E), or V γ 9+ γ δ (H) T cells expressing CD107a or granzyme B.

(C, F) The composition of the total T cell response captured for each BCG dose group was characterized as the relative proportion of antigen-stimulated cells producing every combination of CD154, IFN γ , IL-2, and TNF, with or without IL-17 (CD4, C) or any combination of IFN γ , IL-2, and TNF (CD8, F). Bar graphs show the frequency of memory CD4 or CD8 T cells in PBMC producing cytokines in response to WCL at the peak of the immune response (4 weeks). Responses from individual macaques (symbols) are shown with interquartile range (bar) and median (horizontal line). Pie graphs represent the average proportion of total cytokine production at peak comprising each cytokine combination for each IV BCG dose group; the proportion of the total response producing IL-17 at peak (C, right) is indicated with a black arc (pies) for CD4 T cells only.

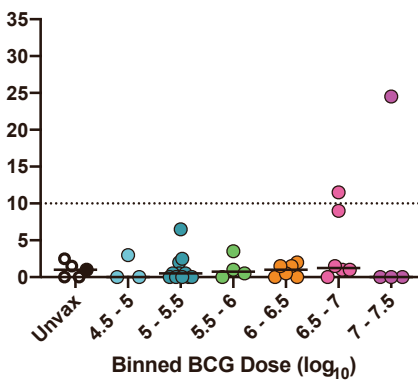
Figure S10

A

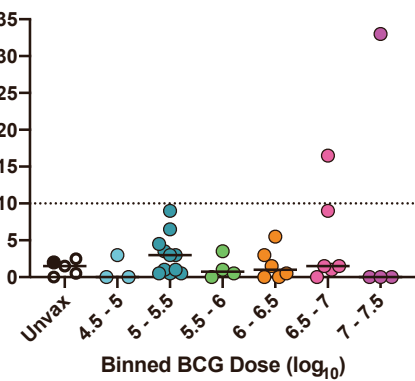
ESAT-6 Pre-Mtb



CFP-10 Pre-Mtb



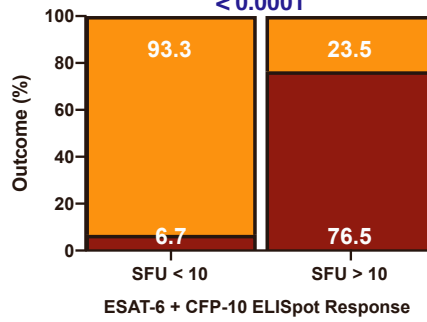
ESAT-6 + CFP-10 Pre-Mtb



B

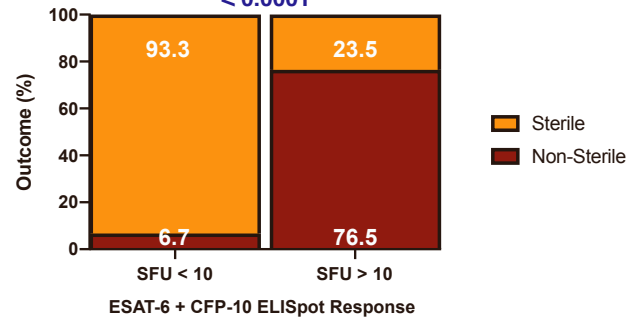
Lung Sterility

< 0.0001



Lung Lymph Node Sterility

< 0.0001



C

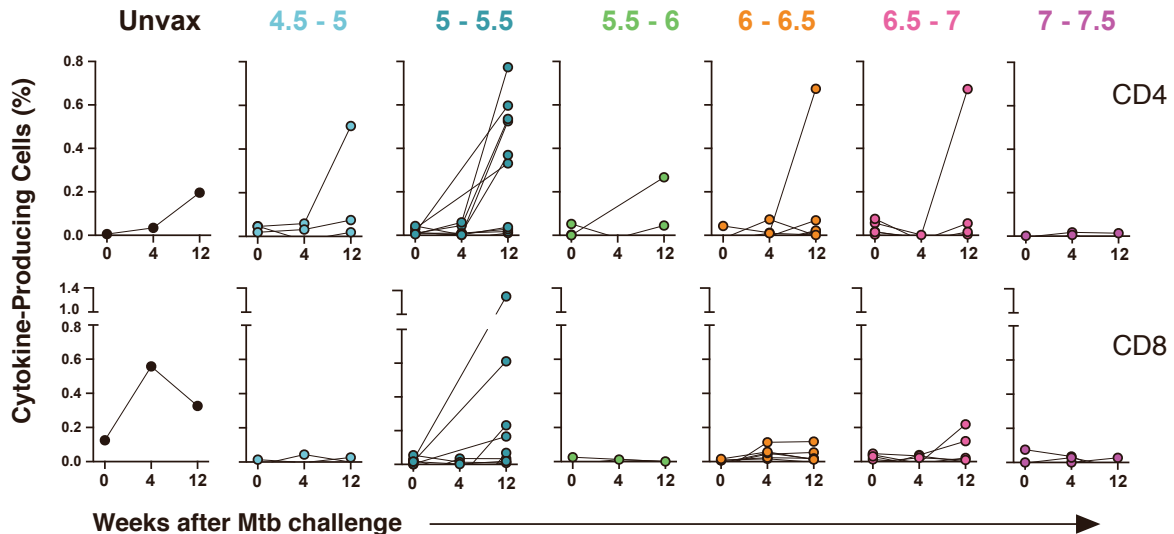


Figure S10. Mtb-specific responses prior to and after Mtb infection in IV BCG vaccinated macaques, related to Figure 5.

(A) Pre-challenge PBMC responses against antigens found in Mtb (but not BCG), ESAT-6, CFP-10, or ESAT-6 + CFP-10 peptides combined, as determined by IFN γ ELISpot. Symbols represent individual animals; horizontal solid bars represent the median; dashed horizontal line represents the SFU cut-off at which at least 95% of uninfected animals fall for each antigen.

(B) Outcome (%) of macaques with sterile or non-sterile lung or lung lymph nodes (i.e., 0 Mtb CFU) that are either positive (> 10 SFU) or negative (< 10 SFU) by ESAT-6 + CFP-10-responsive IFN γ ELISpots. Fisher's exact test p-value reported (two-sided).

(C) Frequency of memory CD4 (top) or CD8 (bottom) T cells producing IFN γ , IL-2, TNF, or IL-17 in response to ESAT-6 + CFP-10 peptides for individual animals in each binned dose group at 0-, 4-, and 12-weeks post Mtb-challenge as measured by flow cytometry.

Figure S11

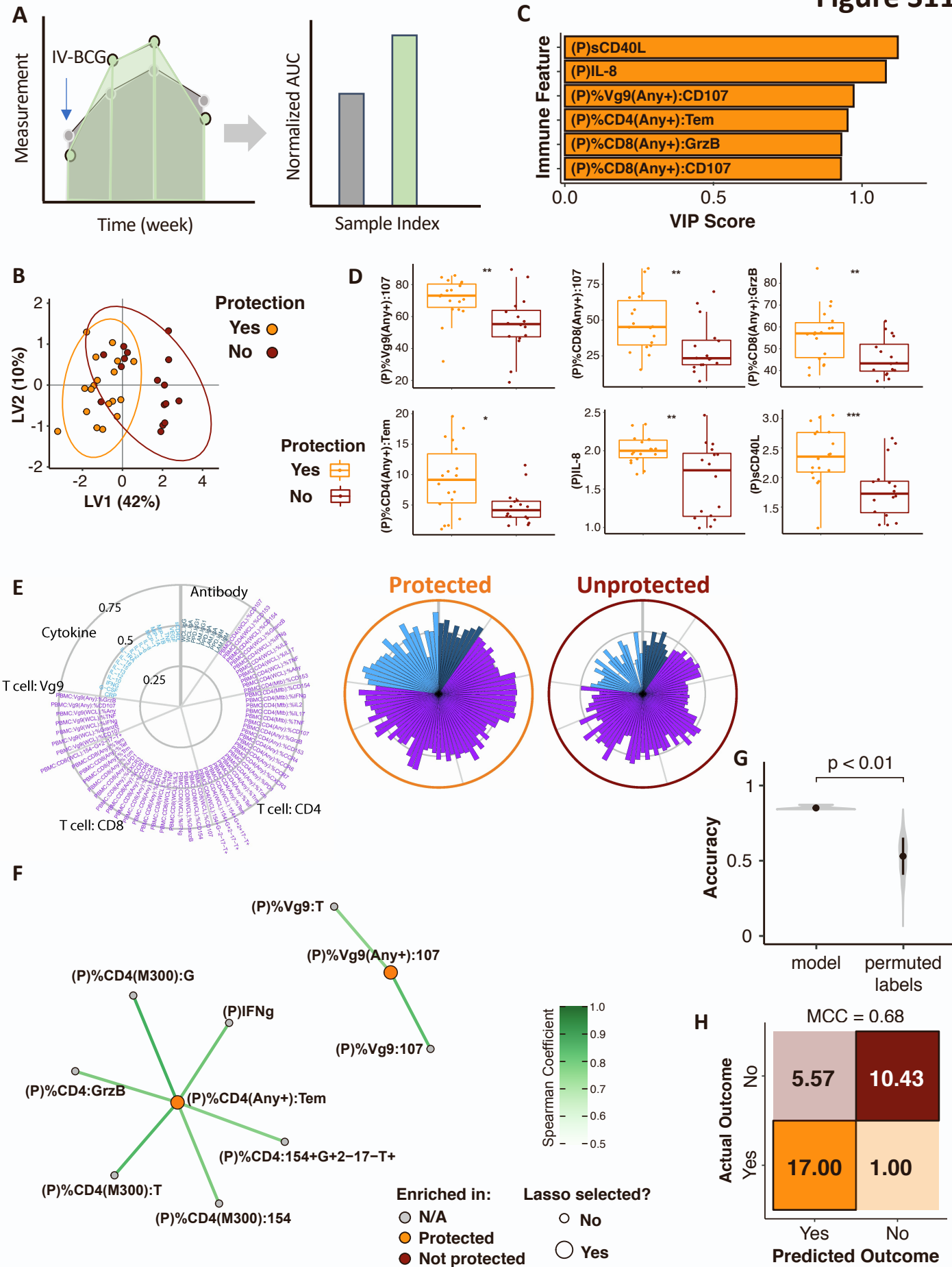


Figure S11. Selected immune features from blood distinguish protected and unprotected macaques, related to Figure 6.

(A) The schematic plot shows the AUC calculation using the temporal profile of each immune measurement.

(B–D) The PLSDA scores plot shows the degree of discrimination of protection achievable following the LASSO selection of immune features from blood **(B)**. Each symbol is one animal, and ellipses indicate 95% confidence regions assuming a multivariate t distribution. **(C)** The bar plot shows the Variable Importance in Projection (VIP) score of the six selected features required to separate the groups (P, PBMC or plasma); the magnitude indicates the importance of the features to group separation and the color of the bar indicates in which group the feature is enriched (higher median value). **(D)** Univariate box plot shows the distribution of each selected feature. Each box represents the IQR (box) with median (bar) and whiskers ($1.5 * \text{IQR}$). * $p < 0.05$, ** $p < 0.01$, *** $p < 0.001$, **** $p < 0.0001$.

(E) Polar plots depict the mean percentile of each measurement across the protected and unprotected groups. The major slices represent the antibody measurements, numbers of different cell types, and numbers or frequencies of T cells with different expressed cytokine expressions. The length of the wedge depicts the mean percentile ranging from 0–0.75 with a step of 0.25.

(F) The correlation network shows the co-correlated features (small grey nodes) that are significantly correlated ($p < 0.05$ after multiple test correction using the Benjamini-Hochberg procedure, Spearman's correlation > 0.7) with the model selected features (large nodes, colored by the protection group in which they are enriched.) See also **Table S3**.

(G–H) The performance and robustness of the model are validated with permutation testing and confusion matrix. The violin plot shows the distributions of repeated classification accuracy testing using label permutation; the p-value is two-sided **(G)**. Black squares indicate the median accuracy and black lines represent one SD. **H)** Average confusion matrix of our PLSDA model. The stratified five-fold cross-validation strategy was applied to the PLSDA model 100 times, Matthews correlation coefficient (MCC).

Figure S12

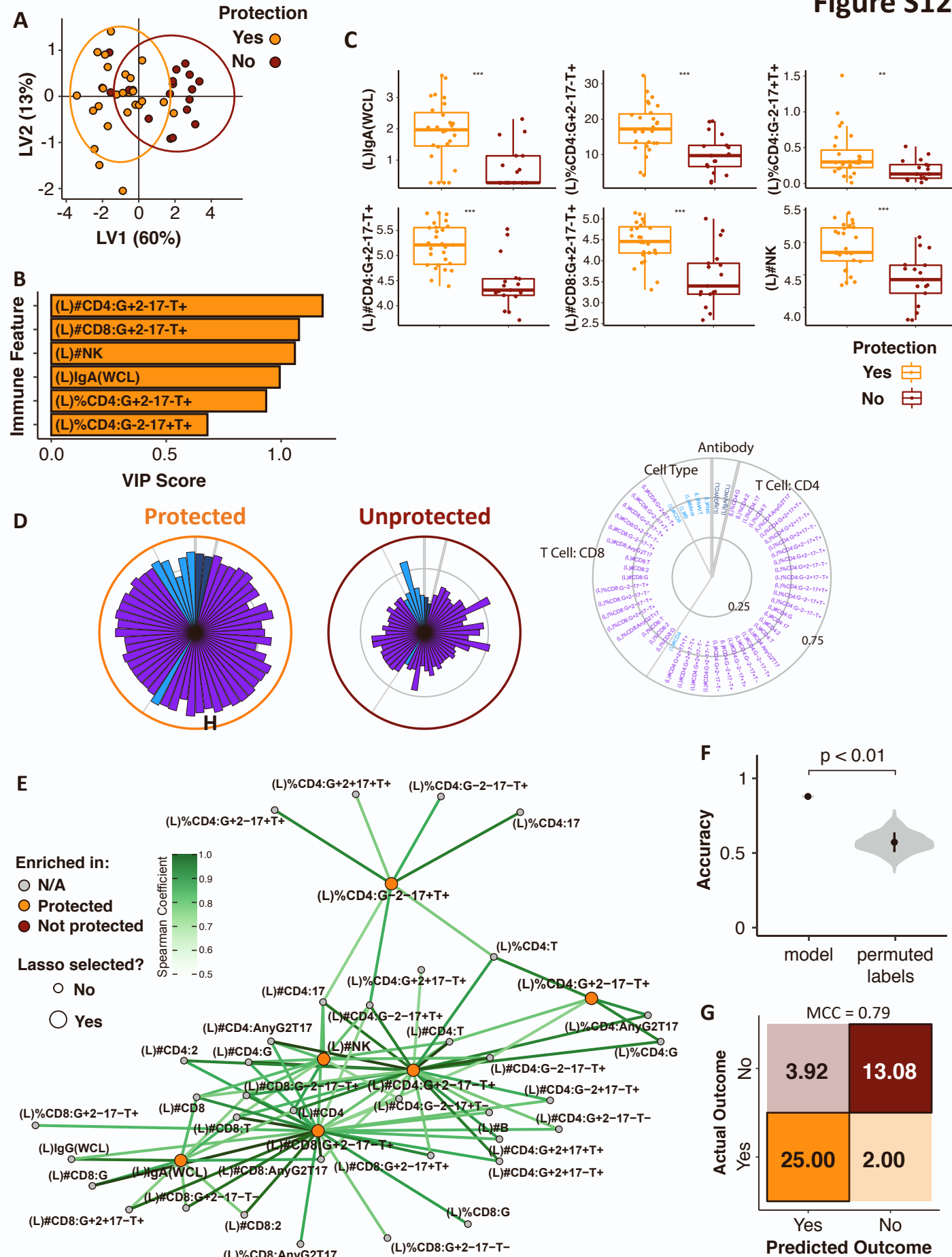


Figure S12. Selected features in BAL from current and historical cohort distinguish protected and unprotected macaques, related to Figure 6.

(A–C) The PLSDA scores plot shows the degree of discrimination that is achievable across the groups following the LASSO feature selection. Each symbol is one sample, and ellipses indicate 95% confidence regions assuming a multivariate *t* distribution (A). The bar plot (B) shows the VIP score of the six selected features in BAL (L, lung) required to separate the groups; the magnitude indicates the importance of the features to group separation. The bar color indicates in which group the feature is enriched (higher median value). Univariate Box plots (C) show the distribution of each selected feature. Each box represents the IQR with median (central line) and whiskers (1.5 * IQR). * $p < 0.05$, ** $p < 0.01$, *** $p < 0.001$, **** $p < 0.0001$.

(D) Polar plots depict the mean percentile of each measurement across the protected and the unprotected groups. The major slices represent the antibody related measurements, cell type measurements and T cell measurements with different expressed cytokine expressions. The length of the wedge depicts the mean percentile ranging from 0–0.75 with the step of 0.25.

(E) The correlation network shows the co-correlated features (small grey nodes) that are significantly correlated ($p < 0.05$ after Benjamini-Hochberg correction, Spearman's correlation > 0.7) with the model selected features (large nodes colored by the protection group in which they are enriched). See also **Table S3**.

(F) The performance and robustness of the model are validated with permutation testing and confusion matrix. The violin plot shows the distributions of repeated classification accuracy testing using label permutation with two-sided *p*-value (F). Black squares indicate the median accuracy and black lines represent one SD. **(G)** Average confusion matrix of our PLSDA model. The stratified five-fold cross-validation strategy was applied to the PLSDA model 100 times; Matthews correlation coefficient (MCC).

Table S2. Logistic Regression Analysis of Protection

Predictor	β	SE β	Wald's χ^2	<i>p</i>	Lower 95%	Upper 95%	Odds Ratio
Intercept	-4.0741	3.7536	1.1800	0.2778	-12.0539	3.2383	
IV BCG Dose (\log_{10})	-0.5862	0.8347	0.4900	0.4825	-2.4194	0.9833	0.5564
CD4 (% Ag-specific)	0.2357	0.0908	6.7400	0.0095	0.0900	0.4563	1.2659
Overall model evaluation		<i>DF</i>	χ^2	<i>p</i>			
Likelihood ratio test		2	20.8189	<.0001			
Predictor	β	SE β	Wald's χ^2	<i>p</i>	Lower 95%	Upper 95%	Odds Ratio
Intercept	-7.5460	3.2005	5.5600	0.0184	-14.5388	-1.7506	
IV BCG Dose (\log_{10})	1.2869	0.5785	4.9500	0.0261	0.2393	2.5559	3.6216
CD8 (% Ag-specific)	-0.0040	0.1376	0.0000	0.9771	-0.2581	0.3000	0.9961
Overall model evaluation		<i>DF</i>	χ^2	<i>p</i>			
Likelihood ratio test		2	7.8045	0.0202			
Predictor	β	SE β	Wald's χ^2	<i>p</i>	Lower 95%	Upper 95%	Odds Ratio
Intercept	-18.4119	5.8343	9.9600	0.0016	-32.2591	-8.6427	
IV BCG Dose (\log_{10})	-0.6791	0.8684	0.6100	0.4342	-2.5168	0.9816	0.5071
CD4 (# Ag-specific \log_{10})	4.3572	1.6278	7.1600	0.0074	1.5570	8.1328	78.0348
Overall model evaluation		<i>DF</i>	χ^2	<i>p</i>			
Likelihood ratio test		2	18.2412	0.0001			
Predictor	β	SE β	Wald's χ^2	<i>p</i>	Lower 95%	Upper 95%	Odds Ratio
Intercept	-10.0320	3.8318	6.8500	0.0088	-18.7101	-3.3058	
IV BCG Dose (\log_{10})	0.5955	0.7179	0.6900	0.4068	-0.8233	2.0601	1.8139
CD8 (# Ag-specific \log_{10})	1.4740	1.1092	1.7700	0.1839	-0.5861	3.9090	4.3666
Overall model evaluation		<i>DF</i>	χ^2	<i>p</i>			
Likelihood ratio test		2	9.7368	0.0077			

Table S2. Logistic regression analysis of protection, related to Figures 1 and 5.

Logistic regression analysis using peak frequencies and numbers of cytokine-producing memory CD4 and CD8 T cell frequencies and numbers from BAL, with IV BCG dose as fixed predictor variables. Each logistic regression model shows predictor name in first column with parameter estimate (β), standard error of parameter estimate (SE β), Wald Chi-Square test statistic (Wald χ^2), p-value for Wald test (p), lower and upper 95% confidence interval bounds for parameter estimate, and an odds ratio. Each model was evaluated using a likelihood ratio test and degrees of freedom (DF), Chi-Square test statistic (χ^2) and p-value for likelihood ratio test are reported. Predictor p-values are highlighted in bold text. If a p-value is statistically significant (less than 0.05), the corresponding odds ratio is highlighted in bold text.